Dynamics of a Convectively Unstable Atmosphere: Jupiter?

GARETH P. WILLIAMS AND JOHN B. ROBINSON

Geophysical Fluid Dynamics Laboratory, NOAA, Princeton University, Princeton, N. J. 08540

(Manuscript received 12 May 1972, in revised form 21 December 1972)

ABSTRACT

We test the hypothesis that the atmospheric circulations of Jupiter are a manifestation of large-scale convective instability brought about primarily by the presence of an internal heat source. This is done by examining the nature of convection in an unstable rotating atmosphere through numerical integration of the Boussinesq equations. The general properties of convection are obtained from solutions with laboratory-scale parameters while particular Jovian characteristics are studied through calculations with planetary-scale parameters.

In the Jupiter calculations, physical and theoretical constraints on parametric freedom produce a desirably under-determined system in which there remain more observational criteria to be explained than free parameters to manipulate.

The solutions indicate that a tropical westerly jet can be produced by an axisymmetric flow provided that the atmosphere is relatively shallow ($d<500$ km). A strong equatorial westerly flow can occur provided that there is a strong diffusion of the tropical jet. The strength of such a diffusion is of a magnitude that suggests that it can only realistically be brought about by large-scale non-axisymmetric disturbances. The axisymmetry of the convective rolls, i.e., their longitudinal stability, is controlled by the latitudinal variation of $\Omega \cos\theta$. This differential rotation suppresses the organization of large-scale convective motion poleward of 45° while toward the equator such motions can set in strongly.

The banded structure and zonal velocity field of the most realistic theoretical solution resemble the observed, having five zones ($w>0$) and four belts ($w<0$) each with its characteristic differential zonal motion. The square-shaped form of the mean vertical velocity variation with latitude produces sharply bounded zones of uniform intensity.

Calculations to test the stability of the axisymmetric flow to longitudinal perturbations indicate that ovals and streaks are the natural form of the disturbance elements.

1. Introduction

The question of whether an atmosphere can be statically unstable everywhere and yet organize itself into a large-scale flow pattern appears to be a basic problem in understanding the circulations on Jupiter and in the Earth's tropics. We would like to examine this problem by deriving the possible character of an unstable atmosphere and then by using the observed Jupiter flow in a positive comparison, suggest its existence.

In any study relating to a remote planetary atmosphere, the level of inquiry and understanding pursued must depend upon two major considerations: 1) the observational data and 2) the governing physical laws. Both items are equally important, since physical simplicity can compensate for limited data and perhaps allow a reasonable understanding of a remote atmosphere to be attained. In particular, the orderliness (i.e., the axisymmetry) of the Jovian cloud systems is suggestive of an underlying simplicity in the dynamics of that atmosphere that might permit such an understanding at this time. With this in mind, our investigation will take the simplest possible form and will be more in the nature of examining the classification and structure of basic dynamical mechanisms than of a planetary simulation.

It would provide a simplifying reduction and generalization of planetary atmosphere theory if the atmospheric circulation systems of the planets could be classified into some simple scheme, just as stars and galaxies can be placed within a few spectral categories. We would like to suggest that two basic broad categories of planetary dynamical systems may be possible. These, for lack of better terminology, we shall refer to as the *baroclinic* and *convective* systems. By a *baroclinic* system we denote a system whose physical behavior is primarily determined by the need to transfer heat horizontally from hot to cold regions. Such a system is associated with a horizontal (potential) temperature differential driving the motions so that the system may be denoted (partly schematically) by the symbol $\Delta_H T$. A convective system specifies a planetary atmosphere where the primary need is to transfer heat upward to higher levels and may be denoted by a positive vertical (potential or equivalent[1] potential) temperature differential symbol $\Delta_V T$. Various fluid dynamical modes can exist within both categories. A fundamental difference between the

[1] When condensation effects are important.

two systems lies in the form of their turbulence fields with the result that different degrees of predictability may be expected.

Limited laboratory analogs of the baroclinic and convective categories occur, respectively, in the well-known Hide (annulus) and Bénard (with rotation) experiments. Because of the simple boundary conditions in these experiments, their flows can also be quantitatively classified in terms of the Richardson, Rossby and Taylor numbers or the Rayleigh and Taylor numbers. On the planetary scale we are familiar with the baroclinic system in the Earth's extratropical dynamics. Despite large topographical influences the Earth's ocean and the Martian atmosphere may also be essentially baroclinic. Venus has an intricate circulation (Rivas, 1971), but is nonetheless baroclinic, being driven by a complex $\Delta_H T$. However, it has not yet been established that a convective system can exist on a planetary scale,[2] even though there is evidence for it on the solar scale. Thus, it is the purpose of this paper to hypothesize such a system and to evaluate the consequences.

Attempts to categorize planetary atmosphere behavior are implicit in the recent papers of Golitsyn (1970) and Stone (1972a). Golitsyn's derivation of similarity parameters for the radiative-dynamical systems of the planets provides a classification of atmospheric energetics that may be too complex to verify with the small observational sample available. Stone's paper involves the derivation of "a theory for the static stability" of rotating planetary atmospheres and concentrates on atmospheres where the baroclinic instability mechanisms could predominate. Such a theory could provide a more exacting baroclinic classification. Stone's theory, however, cannot provide a complete specification of a planetary atmosphere for its assumptions are invalid, for example, for the Earth's tropical circulation. To classify a particular atmosphere requires that the relative importance of the two basic thermal influences, $\Delta_H T$ and $\Delta_V T$, and their associated sources of available potential energy be evaluated. Stone's (1972a) analysis covers the case where the baroclinic forcing $\Delta_H T$ can be assumed to dominate. He then seeks the associated $-\Delta_V T$. We suggest that it is also necessary to consider flows in which $\Delta_V T$ dominates and for which a dependent $\Delta_H T$ can be evaluated if desired.

The Earth's atmosphere, being baroclinic in extratropical regions and probably convective in the tropics, falls into a hybrid category. It is not clear that the tropical circulation is primarily a statically stable circulation driven by the tropical $\Delta_H T$ or is a large convective cell driven by conditional convective instability. The tropics may be equally influenced by both ΔT effects and be too idiosyncratic to be a good example of any basic dynamical mechanism.

[2] Except perhaps in a highly specialized form in the ITCZ.

Thus, only on Jupiter and Saturn does it appear that we could have a manifestation of a simple convective atmosphere. The alternative possibility, that Jupiter's circulation could be explained by a baroclinic mechanism, was first suggested by Stone (1967) and Gierasch and Stone (1968) but Stone's (1972b) later analysis has narrowed down, almost to the point of exclusion, the possibility that the inertial mode could produce an equatorial jet.[3] Other authors [notably Lau (1913), Wasiutynski (1946) and Hide (1969); also see Gierasch (1970)] have pointed out the morphological similarity between the banded structure of Jupiter and that obtained in certain laboratory experiments on Bénard convection. Clearly, a convective mode should be favored in a system with a dominant internal heat source (Jupiter) or in a system which behaves as if it was heated from below due to its transparency to solar radiation (Earth's tropics?). However, the existence of such a mode on a planetary scale has not been established.

The fact that Jupiter has an interior heat source that exerts a predominant influence on its atmospheric circulation is loosely suggested by a comparison of the simple observation features of Jupiter and Saturn, as follows. First, consider the similarities of the two atmospheres: 1) axisymmetric banded structure, 2) strong equatorial jets, and 3) comparable physical configuration [rotation rate, high albedo (0.6), small orbit eccentricity]. Second, consider the dissimilarities between the two planets: 1) the equatorial inclinations are 3° for Jupiter and 27° for Saturn, and 2) Saturn receives one-fourth as much solar radiation as Jupiter but its jet is four times stronger. Now the dissimilarities are with respect to the solar influence which suggests that the similarities, i.e., the dynamical system, can have little correlation with the solar influence and must be primarily determined by internal heating. The absence of any apparent seasonal variations in the strongly inclined Saturn atmosphere points to a weak solar influence and the strength of Saturn's jet compared to Jupiter's would seem to be more easily explainable by the presence of an internal energy source [possibly larger than that observed by Auman *et al.* (1969)]. Although such arguments based on indirect evidence are ambivalent if the flow structure is unknown, quantitative estimates of the Jovian internal heat sources from the observed effective temperatures do put their values at about 3/2 times as strong as the solar supply (Aumann *et al.*; Trafton and Wildey, 1970).

The best confirmed features of the Jovian motions that require a theoretical explanation are those that have been observed long enough to have a climatological significance. The phenomena, documented by Peek (1958), are as follows:

[3] However, a numerical investigation of this mode is required for completeness.

1) The axisymmetric, to first order, banded structure and uniform polar regions.

2) There is a differential rotation within zones (light color) and belts (dark color) such that positive zonal motion is associated with the equatorward edges of belts (poleward edges of zones) and negative zonal motion with the poleward edges of belts (equatorward edges of zones). The correlation between zones and belts and the upper and lower levels of the atmosphere and then perhaps with vertical motion is unknown. The consensus opinion seems to be that the zones are upper level clouds whereas the belts relate to a deeper level in the atmosphere. The cloud layer models of Lewis (1969) suggest that clouds may be expected at three different levels in our region of interest: NH_3 at 150K, NH_4HS at 225K and H_2O at 275K, and that the region between the top and bottom clouds ($\sim$80 km) is convective.

3) There is a strong positive equatorial zonal motion of $\sim$100 m sec^{-1}. A more detailed analysis of the observations by Chapman (1969) has provided an estimate of the variation of the upper level zonal velocity with latitude.

4) The shape of the disturbances, i.e., deviations from the axisymmetric structure is well known and seems to be dominated by the white ovals.

5) The Great Red Spot.

The calculations made to investigate the form of a convective atmosphere and its relation to the Jovian system are presented in four sections. The simplest question is asked first, that is, how do sphericity and rotation affect the well-known Bénard convection characteristics? To answer this, solutions are obtained in Section 3 that describe Bénard convection on a rotating sphere for laboratory scale values. Then it is shown in Section 4 how such convection can be produced for a planetary-scale shallow atmosphere by the use of eddy viscosities. In that section it will also be shown how a tropical jet can be produced and how the shape of the jet allows the depth of the atmosphere to be estimated.

In Section 5 more specific Jupiter-related calculations are made to derive the closest matching solution to the observed data. We are then led in Section 6 to examine a basic problem that must be surmounted in understanding a convective atmosphere, i.e., how do we correctly parameterize turbulent convection on a planetary scale? This is a most difficult question for no good theoretical links between linear Bénard theory and the study of thermal turbulence. The only links available are the concepts of eddy diffusion and mixing-length theory and in Section 6 the latter is exploited in the form of nonlinear viscosities in an attempt to deal with this problem.

2. The mathematical model

The system of equations to be integrated represents a highly idealized system. Both the incompressible and Boussinesq assumptions are made to provide a simple mathematical system that is convenient for calculations over a wide range of parameter values. Although these approximations inhibit a direct simulation of or accurate quantitative comparisons with Jupiter, the Boussinesq system does provide the lowest level of model that can produce most of the important modes expected to occur in the Jovian atmosphere. By proceeding from the simplest models we can hope to obtain an understanding of possible later simulations. Such was the approach in the evolution of the understanding of the Earth's global circulation from Eady's (1949) simple incompressible Boussinesq model to later simulations. Simple abstract models have the advantage of generality, so that their basic modes are of interest in themselves even if they should prove to be irrelevant to the particular natural phenomenon under discussion. The equations are also applied outside the intended range of the Boussinesq approximation but it is believed that the resulting distortions are quantitative, not qualitative.

To construct an elementary planetary model, simple but universal boundary conditions on the thermal field are desirable. Either T or T_z may be specified, both forms being general. For simplicity and precision in providing a fixed ΔT for evaluating parameters, it appears more appropriate to specify T. In observing a planet, T rather than T_z is most likely to be observed so such a condition is also appropriate for application. The T and T_z conditions correspond to assuming infinite heat capacity (ocean-like) and finite heat capacity (land-like), respectively, for the interface. For internal heating the T condition seems more appropriate.

Thus, we consider the motion of an incompressible fluid bounded by a spherical shell of inner radius a and outer radius $a+d$. The fluid is subject to a gravitational force acting toward the center of the spheres. The inner sphere rotates with a uniform rate Ω. Motion relative to the solid rotation of the system is measured in spherical coordinates (r,θ,ϕ), where r is radial distance, θ the co-latitude measured from the Pole, and ϕ the azimuthal angle (longitude). The velocity components are u, v, w in the zonal, co-latitudinal and vertical directions, respectively.

The Boussinesq fluid is defined as being such that density variations are negligible except in the buoyancy term, and that the coefficients ν, κ, β of viscosity, heat diffusivity[4], and thermal expansion are constant. The centrifugal acceleration is taken to be negligible compared with gravity as a consequence of which we can take the outer sphere to be a free-slip rigid lid surface of constant height for the fluid. [However, the oblate-

[4] Apart from the mixing-length formulation of Section 6.

ness of Jupiter is relatively large (1:15) and its effects, although secondary, should be investigated.]

The inner and outer spheres are taken to be perfectly conducting and held at different constant temperatures T_1 and T_2, respectively. The imposed radial temperature differential $\Delta T = T_1 - T_2$ drives the fluid away from a state of solid rotation. The lateral boundaries (usually at the pole or 45° latitude and the equator) are assumed to have no heat flow across them. Most of the calculations are made for a hemispheric domain. This system forms the classical Bénard problem for a spherical shell (see, e.g., Chandrasekhar, 1961).

In forming the equations of motion considerable simplification is afforded if the radius a replaces the variable r when undifferentiated. This procedure is accurate for shallow fluid layers, i.e., when $d \ll a$. Taking $r = a + z$, the equations of motion with $r \to a$ may be written as

$$\frac{Du}{Dt} = -\frac{p_\phi}{a \sin\theta} - \left(2\Omega + \frac{u}{a \sin\theta}\right)[v \cos\theta + (\omega \sin\theta)^*] + F_u, \quad (1)$$

$$\frac{Dv}{Dt} = -\frac{p_\theta}{a} + \left(2\Omega + \frac{u}{a \sin\theta}\right) u \cos\theta - \left(\frac{vw}{a}\right)^* + F_v, \quad (2)$$

$$\frac{Dw}{Dt} = -p_z + \beta g T + \left(\frac{v^2}{a}\right)^* + \left[2\Omega + \frac{u}{a \sin\theta}\right](u \sin\theta)^* + F_w, \quad (3)$$

with the heat transfer equation as

$$\frac{DT}{Dt} = F_T, \quad (4)$$

and the equation of mass conservation as

$$w_z + \frac{1}{a \sin\theta}(v \sin\theta)_\theta + \frac{u_\phi}{a \sin\theta} = 0, \quad (5)$$

where we have used the operator identity

$$\frac{Dq}{Dt} \equiv q_t + \frac{v}{a} q_\theta + \frac{u}{a \sin\theta} q_\phi + w q_z. \quad (6)$$

The hydrostatic pressure deviation has been written as $p = p'/\rho_0$ and the temperature deviation from T_2 as T.

The formulation of the shallow atmosphere approximation $r \to a$ to the equations of motion for a fluid has been discussed by Phillips (1966, 1968) and Veronis (1968). It is customary in studies of the Earth's global circulation to omit the terms marked by an asterisk in Eqs. (1)–(3). Phillips (1966) suggested that the omission of these terms was consistent with introducing the shallow atmosphere approximation as a geometric approximation via the curvilinear scale factors and that the resulting system of equations had consistent conservation properties. Veronis, however, indicated the error of such a formalistic approach in that the approximated equations excluded certain dynamical modes. Phillips (1968) then suggested that the approximation could be justified for stable atmospheres such as the Earth's.

As planetary atmospheres need not necessarily be stable, and indeed the opposite is proposed for Jupiter, the asterisk-marked terms will be retained for the planetary-scale calculations. For a very shallow atmosphere the asterisk terms are probably negligible. However, the equations will be applied to relatively deep atmospheres ($d/a \approx 10^{-1}$) in which deep atmosphere effects become active, although secondary. For such calculations the shallow atmosphere approximation is tending toward marginal validity. Because of the inclusion of deeper atmosphere effects in Eqs. (1)–(3), the equations can be considered to form a "semi-shallow" atmosphere approximation. For similar reasons of generality the hydrostatic approximation is not made. The asterisk terms are artificially omitted in the laboratory-scale calculations so that shallow atmosphere type convection can be investigated.

The form of the friction terms $\mathbf{F} = (F_u, F_v, F_w)$ varies for the different calculations. The Navier-Stokes friction form is used for the laboratory-scale calculations (Section 3). The planetary-scale calculations utilize eddy coefficients ν_H and ν_V, where the horizontal coefficient ν_H differs greatly from the vertical (ν_V) because of the different length scales involved. The use of these coefficients is based on the assumption that the turbulence can be regarded as being transversely isotropic. The formulation of such friction terms and their shallow atmosphere approximated form has been discussed elsewhere (Williams, 1972). A more complex form of $\mathbf{F}$ using mixing-length theory to parameterize turbulent convection is discussed later in Section 6.

The following expressions for $\mathbf{F}$ are used in the general planetary-scale convection calculations of Sections 3 and 4:

$$F_u = \frac{\nu_H}{a^2}\left(\nabla_H{}^2 u - \frac{u \cos 2\theta}{\sin^2\theta} + 2v_\phi \frac{\cot\theta}{\sin\theta}\right) + \nu_V u_{zz}, \quad (7)$$

$$F_v = \frac{\nu_H}{a^2}\left(\nabla_H{}^2 v - v \frac{\cos 2\theta}{\sin^2\theta} - 2u_\phi \frac{\cot\theta}{\sin\theta}\right) + \nu_V v_{zz}, \quad (8)$$

$$F_w = \frac{\nu_V}{a^2}\nabla_H{}^2 w + \nu_V w_{zz}, \quad (9)$$

where the horizontal operator

$$\nabla_H{}^2 q \equiv q_{\theta\theta} + q_\theta \cot\theta + \frac{q_{\phi\phi}}{\sin^2\theta}. \quad (10)$$

TABLE 1. Cases computed for laboratory-scale parameters. Constant parameter values are $a=10$ cm, $d=1.5$ cm, $\nu=1.008\times10^{-2}$ cm^2 sec^{-1}, $\kappa=1.42\times10^{-3}$ cm^2 sec^{-1}, $\beta=2.054\times10^{-4}$ (°C)$^{-1}$, $g=981$ cm sec^{-2}. Resolution was $\Delta z'=1/20$, $\Delta\theta'=1/80$. Notation is such that letters A, B, D relate to given Rayleigh number value, integers to the rotation rate (multiplied by 10), and the letter S indicates the use of the varying temperature distribution $\Delta T\sin^2\theta$ along the base, so that the parameters marked with asterisks denote maximum or equatorial values; parameters with daggers are given by the solutions.

Case	ΔT (°C)	Ω (sec^{-1})	R	Ta	d_E	Ro†	Nu†	B_{max}†
A0	0.05	0.0	2376	—	—	—	1.97	—
A1	0.05	0.1	2376	2.0×10^3	0.66	3.9×10^{-3}	1.52	18.3
A2	0.05	0.2	2376	8.0×10^3	0.47	1.8×10^{-3}	1.29	1.1
A2B	0.05	0.2	2376	8.0×10^3	0.47	1.5×10^{-3}	1.30	1.3
A3	0.05	0.3	2376	2.0×10^4	0.38	9.7×10^{-3}	1.20	0.8
A4	0.05	0.4	2376	3.2×10^4	0.33	6.6×19^{-4}	1.14	0.5
A8	0.05	0.8	2376	1.3×10^5	0.23	3.0×10^{-4}	1.04	0.2
A12	0.05	1.2	2376	2.9×10^5	0.19	3.8×10^{-5}	1.001	0.02
B0	0.1	0.0	4751	—	—	—	2.63	—
B2	0.1	0.2	4751	8.0×10^3	0.47	2.1×10^{-3}	1.94	9.8
B4	0.1	0.4	4751	3.2×10^4	0.33	2.0×10^{-4}	1.50	1.7
B8	0.1	0.8	4751	1.3×10^5	0.23	6.8×10^{-4}	1.25	0.9
B16	0.1	1.6	4751	5.1×10^5	0.17	3.4×10^{-4}	1.11	0.3
D0	0.2	0.0	9502	—	—	—	3.27	—
D10	0.2	1.0	9502	2.0×10^5	0.21	9.6×10^{-4}	1.55	1.8
D30	0.2	3.0	9502	1.8×10^6	0.12	3.1×10^{-4}	1.15	0.5
SA0	0.05*	0.0	2376*	—	—	—	1.71	0
SA2	0.05*	0.2	2376*	8.0×10^3	0.47	1.25×10^{-3}	1.37	1.0
SA8	0.05*	0.8	2376*	1.3×10^5	0.23	3.16×10^{-4}	1.06	0.2
SA12	0.05*	1.2	2376*	2.9×10^5	0.19	3.11×10^{-5}	1.001	0.01

These equations reduce to the shallow approximated Navier-Stokes forms if $\nu_H=\nu_V=\nu$ as in Section 3. Horizontal and vertical thermal diffusivities κ_H, κ_V are used for (4) so that

$$F_T=\frac{\kappa_H}{a^2}\nabla_H^2T+\kappa_VT_{zz}. \tag{11}$$

Complex radiative transfers are omitted from (11) in favor of the simpler thermal forcing. In a highly convective atmosphere, heated by the planet's interior, details of the radiation balance of the atmosphere may be of secondary dynamical importance, allowing a simple model to be adequate.

The boundary conditions as used in the calculations to express the state of the fluid at the boundaries are:

On the inner sphere, a state of no slip[5]:

$$w=v=u=0;\quad p_z=\beta gT+\nu_Vw_{zz};\quad T=\Delta T \tag{12}$$

On the outer sphere, a state of free slip:

$$w=u_z=v_z=0;\quad p_z=\beta gT;\quad T=0 \tag{13}$$

At the pole and equator:

$$\left.\begin{aligned} &v=w_\theta=(u/\sin\theta)_\theta=0\\ &\frac{p_\theta}{a}=\left(2\Omega+\frac{u}{a\sin\theta}\right)u\cos\theta\\ &T_\theta=0 \end{aligned}\right\} \tag{14}$$

[5] The complexity of the lower Jovian interface is ignored and idealized as being just a stress bearing surface.

The procedure for solving the system of equations (1)–(14) numerically is discussed in the Appendix. Solutions are obtained as functions of space and time, but we concentrate only on the final steady-state forms. For most of the calculations, axisymmetric solutions are obtained by suppressing the ϕ-dependency in the above equations. This allows examination of more points in parameter space. However, some fully three-dimensional calculations are made to examine the stability of the axisymmetric modes and to examine the character of transient disturbances.

Some pertinent non-dimensional parameters to be calculated are:

(i) Raleigh number $\quad \mathrm{R}=g\beta\Delta Td^3/(\nu_V\kappa_V)$
(ii) Taylor number $\quad \mathrm{Ta}=4\Omega^2d^4/\nu_V^2$
(iii) Rossby number $\quad \mathrm{Ro}=u_{max}/(2\Omega L)$
(iv) Ekman depth ratio $\quad d_E=\pi(\nu_V/\Omega d^2)^{\frac{1}{2}}$
(v) Nusselt number $\quad \mathrm{Nu}=\dfrac{d}{\Delta T}\displaystyle\int_0^{\pi/2}(T_z)_{z=0}\sin\theta d\theta$
(vi) Barotropic stability parameter $\quad B=u_{\theta\theta}/(2\Omega a\sin\theta)$

where $L=a\pi/2$ is taken as the horizontal length scale. Parameters (ii)–(iv) are global parameters which ignore the $\cos\theta$ variation of Ω and must be modified for application to local regions.

3. General properties of shallow-layer convection on a laboratory-scale sphere

To study the general behavior of convective instability in a spherical gravity field it would be informative

to perform laboratory experiments to which we can relate and form concepts under the simplest conditions. This is impossible for the spherical configuration, and experiments in the cylindrical system (Rossby, 1969) are misleading for the spherical context because of the absence of the important $\Omega\cos\theta$ variation. However, hypothetical laboratory experiments can be conducted by numerical integration of the equations for laboratory-scale parameters.

a. Parameter values

The solutions are obtained to describe the flow of water at 20C on a sphere of radius 10 cm with a depth of 1.5 cm for values of the two variable parameters ΔT and Ω listed in Table 1. These parameter values lie in the same range as those of Rossby's (1969) cylindrical system.

For convection in a Cartesian system with one free and one rigid horizontal boundary, theory predicts that instability will arise in a non-rotating system if the Rayleigh number exceeds a critical value of $R_c=1100$ (see, Chandrasekhar, 1961). With rotation present, the critical Rayleigh number increases such that, for example, it is doubled when the Taylor number $Ta=2\times10^3$. Thus, the lowest Rayleigh number cases (set A) were chosen as having a Rayleigh number which lies well but not excessively beyond the $\Omega=0$ critical value. Set A provides the reference set of laboratory-scale solutions.

The effects of increasing the Rayleigh number are examined by doubling and quadrupling the Rayleigh number of set A to give sets B and D. At even higher Rayleigh numbers the convection becomes three-dimensional and calculations for such values are avoided as being inappropriate to the present study.

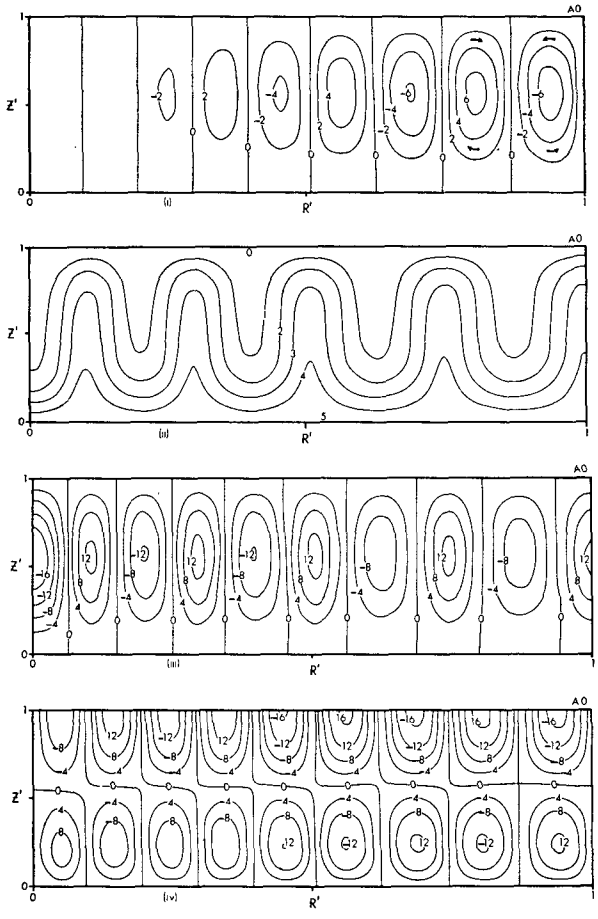

FIG. 1. Case A0: (i) streamfunction $\psi\times10^3$ [cm^2 sec^{-1}] defined as $w\sin\theta=\psi_\theta/a$, $v\sin\theta=-\psi_z$; (ii) temperature $T\times10^2$][°C]; (iii) vertical velocity $w\times10^3$ [cm sec^{-1}]; (iv) meridional velocity $v\times10^3$ [cm sec^{-1}]. Normalized coordinates are $z'=z/d$ and $R'=\theta/(\pi/2)$, the latter going from the pole ($R'=0$) to the equator ($R'=1.0$).

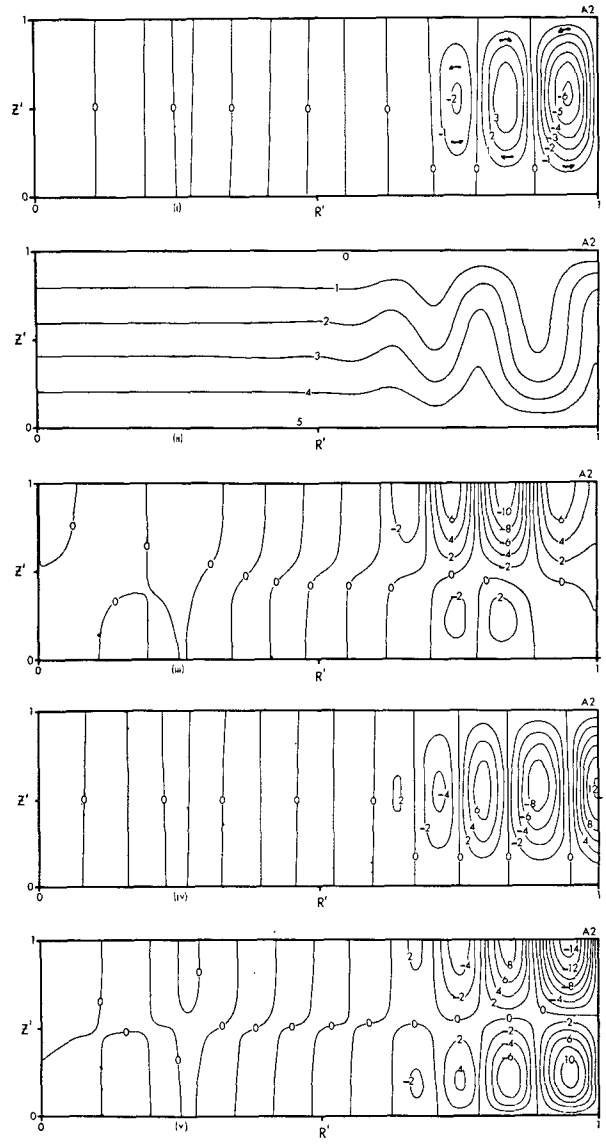

FIG. 2. Case A2: (i) $\psi\times10^3$ [cm^2 sec^{-1}]; (ii) $T\times10^2$ [°C]; (iii) $u\times10^3$ [cm sec^{-1}]; (iv) $w\times10^3$ [cm sec^{-1}]; (v) $v\times10^3$ [cm sec^{-1}].

In each set Ω is increased from zero to examine its effect in limiting the extent of the convection.

To examine how crucial the form of the base temperature distribution is to the type of flow produced, calculations are made with $\Delta T \sin^2\theta$ along the base (set SA). All calculations were made by assuming an initial condition of isothermal fluid at rest. A small random disturbance induces cell development and integrations to steadiness are completed.

b. Equation system

As Bénard cells have an aspect ratio (cell wavelength to depth) of about 3, the overall aspect ratio L/d cannot be made too large or a large number of cells would occur. To examine such a system would be computationally extravagant and, as we shall see later, of less relevance to Jupiter. To yield a reasonable number of cells requires $L/d \approx 10$.

However, for $L/d=10$, although the $d \ll a$ approximation is still valid, the equatorial region of influence (defined by the angle at which the tangent to the inner sphere at the equator intersects the outer sphere) is large ($\sim 25°$). While such a configuration can produce convection of interest (for deep solar atmospheres perhaps) its form[6] is not related to planetary-scale convection with its small equatorial region of influence.

This problem may be circumvented and the above parameter values used to provide laboratory-scale experiments to shallow planetary-type convection, provided that the prediction equations are modified to exclude the influence of the equatorial or deep atmosphere type terms, i.e., $\Omega \sin\theta$ and related terms marked by asterisks in Eqs. (1)–(3). Thus, these terms are suppressed for the laboratory-scale calculations of this section.

[6] With rolls aligned parallel to the rotation axis.

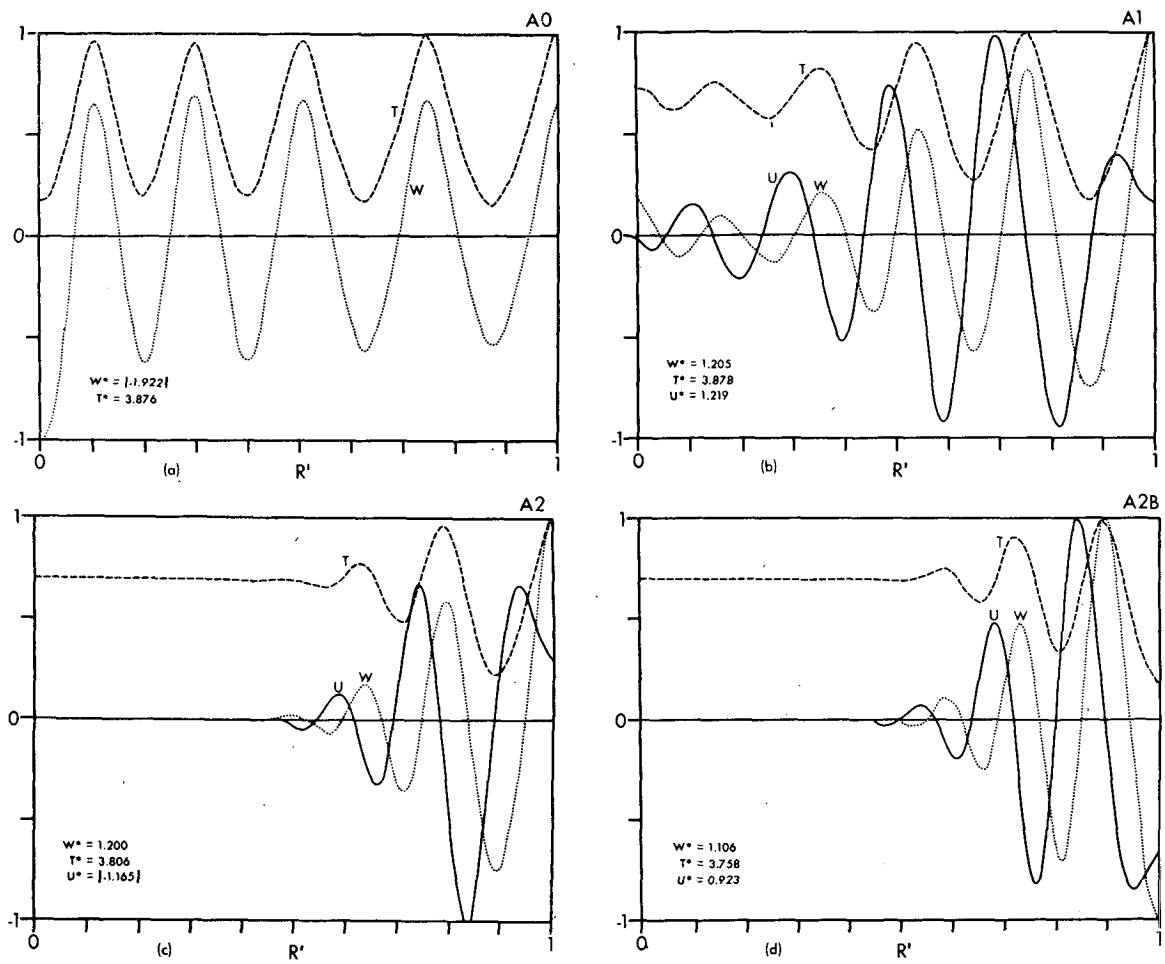

FIG. 3. Set A latitudinal profiles of normalized zonal velocity $u=u/u^*$ [cm sec^{-1}] at $z=d$, normalized vertical velocity $w=w/w^*$ [cm sec^{-1}] at $z=d/2$, and normalized temperature T/T^* [°C] at $z=d/2$. Variables are normalized with respect to their extrema so that they never exceed ± 1. Normalizing constants w^*, u^*, T^* are in units of 10^{-2}. Normalizing constants are shown as moduli of negative values when extremum is a minimum; otherwise, it is a maximum. Part (i) refers to the first set of four panels, part (ii) to the second.

c. Discussion of solution set A

For a given set of parameters, two steady-state solutions are possible for flow in a hemisphere, each differing from the other by a half wavelength. The solution with upflow at the equator will be defined as the *positive* solution and that with downflow as the negative solution. In a global domain of integration, anti-symmetric modes can also arise (see Section 5). For this section the discussion will concentrate on the positive hemispheric (symmetric) mode.

The contours of two typical solutions, A0 and A2, one without rotation and one with, are given in Figs. 1 and 2. The convection in A0 is fairly uniform with latitude $R'=\theta/(2\pi)$ even though the streamfunction, reflecting mass transport, decreases with increasing latitude.[7] The presence of rotation (Fig. 2) suppresses convection in higher latitudes because with the higher local Taylor number in higher latitudes the critical Rayleigh number exceeds the imposed Rayleigh number there. Thus, convection is favored in the equatorial region.

[7] In a non-rotating system the axis of symmetry is arbitrary if rolls exist, as the system has no preferred direction.

Although convection is limited to the equatorial half of the hemisphere in Fig. 2, a comparison with Fig. 1 indicates that the amplitude and shape of the equatorial cell is unchanged by the rotation. The zonal flow produced by the rotation [Fig. 2 (iii)] has a progression at the equator for this positive solution and a regression poleward of it, at upper levels. The regions of alternating positive and negative zonal velocity jets are produced by the thermal wind balance.

To display the remaining results concisely, latitudinal profiles of u at $z=d$ and w, T at $z=d/2$ are presented in Figs. 3–6. The complete flow patterns are similar to those in Figs. 1 and 2. The reference set A (Fig. 3) illustrates most thoroughly the effect that increasing Ω has upon convection. When $\Omega=0.1$ (case A1) the maximum Taylor number of 2×10^3 (at the pole) is associated with a critical Rayleigh number whose value is close to that imposed. Thus, in this case rotation just suffices to dampen but not eliminate the convection in the polar half of the hemisphere. As Ω is increased to 0.2 and 0.3, convection is suppressed in the polar region and damping is extended toward lower latitudes. When

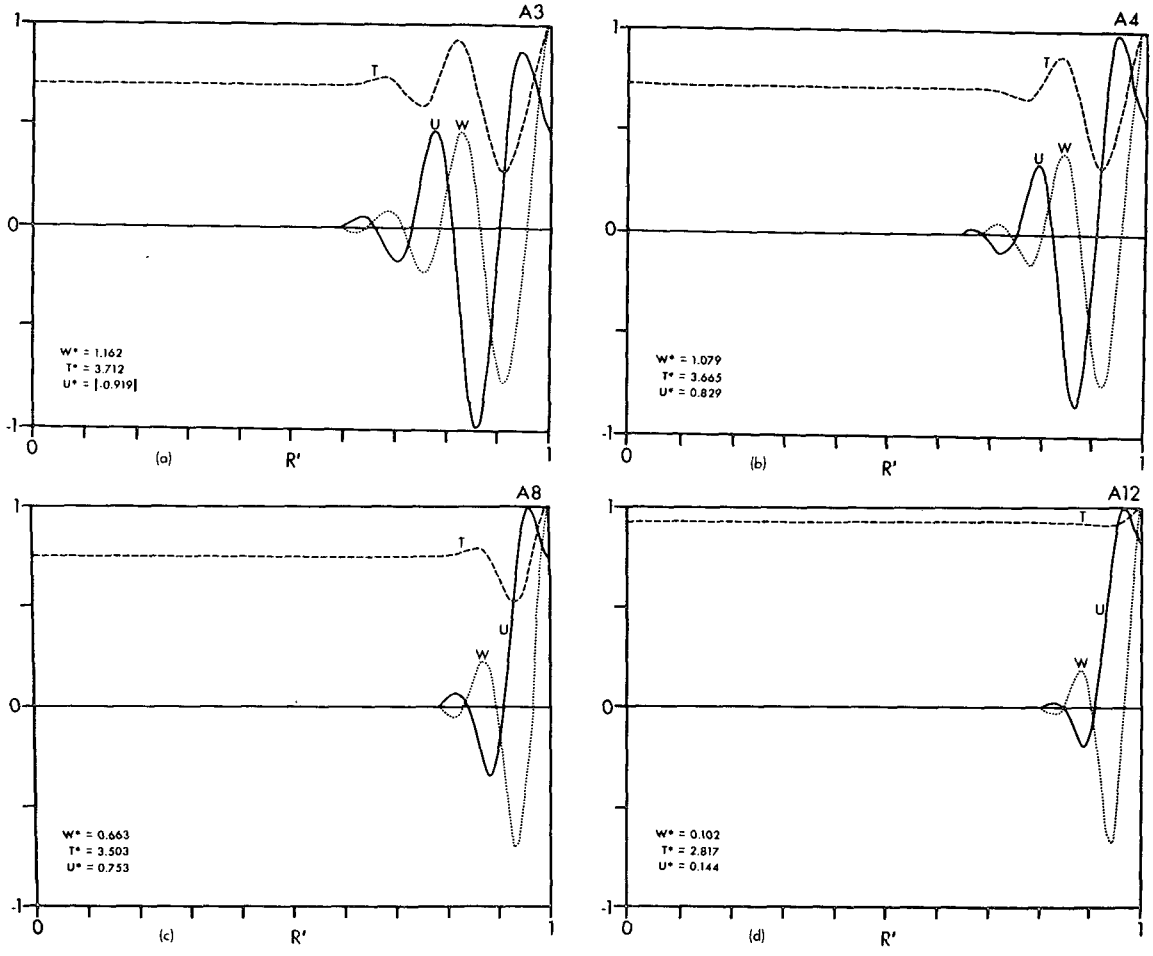

FIG. 3. (*continued*).

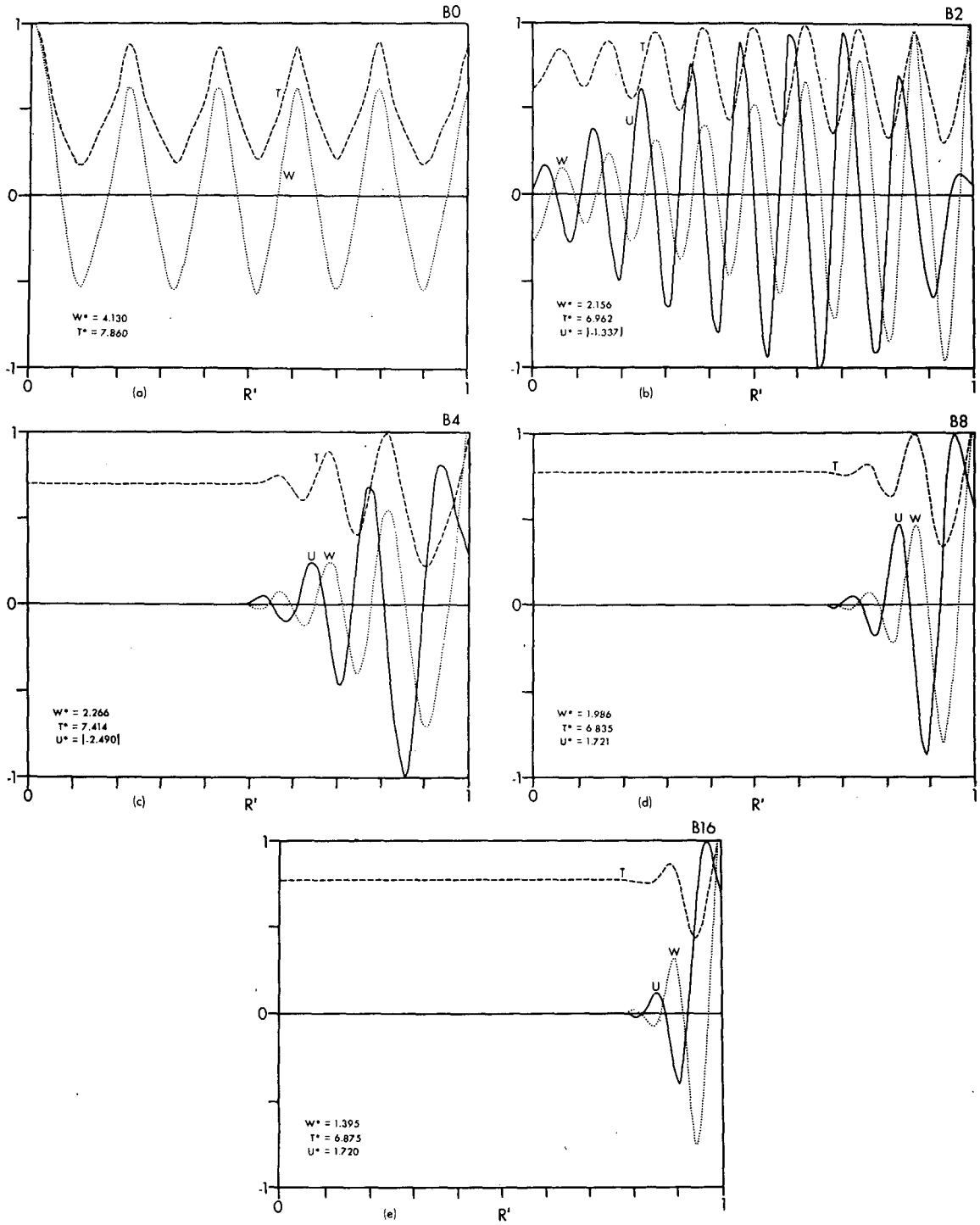

FIG. 4. Set B latitudinal profiles. Legend and units as in Fig. 3.

Ω is raised to 0.4 (case A4) the equatorial progression becomes a stronger zonal flow than its adjacent regression and a further increase of Ω to 0.8 makes the zonal motion a predominantly positive equatorial flow. The maximum amplitudes of the variables do not vary much with rotation when $\Omega<0.8$. However, increasing Ω to 1.2 does not alter the basic flow pattern reached in A8 but the amplitude does become greatly diminished. This indicates that the flow always consists of at least one equatorial cell, never anything less, but that the ampli-

tude of this cell gradually decreases with increasing Ω to reach complete flow extinction.

Fig. 3(i)d indicates that the negative solution A2B has a similar latitudinal range but a weaker amplitude than the corresponding positive solution A2.

d. Discussion of solution sets B *and* D

Increasing the Rayleigh number through values of ΔT produces solutions (sets B and D, in Figs. 4 and 5) similar to those of set A. The contours in the $\Omega=0$ case D0 display a different shape to those of A0 and B0, indicating the presence of greater nonlinear activity as the Rayleigh number increases toward values that produce three-dimensional convective elements.

Comparing the three sets of solutions shows, for example, that cases A8, B16 and D30 have similar distributions and activity ranges. The amplitudes of their variables vary approximately as ΔT and the latitudinal range of activity as $\Delta T/\Omega$, i.e., as $R/Ta^{\frac{1}{2}}$. Thus, whereas Ω affects mainly the range of activity, ΔT determines both the range and amplitude of the convection.

The shape of the equatorial progression does not alter over the parameter range of the solutions. Neither does the size of the cells change very much with increasing Rayleigh number. The Rossby number is slightly lower than that observed for Jupiter.

e. Discussion of solution set SA

Specifying a latitudinal temperature variation $\Delta T \sin^2\theta$ along the base introduces a θ-varying Rayleigh number. In the non-rotating case SA0 (Fig. 6) the Rayleigh number has a value close to the 1100 critical value at $R'=0.5$ so that convection only occurs in the $R'=0.5$–1.0 range.

In cases with rotation, the latitudinal temperature variation produces an additional positive zonal motion in the subcritical region through the thermal wind balance. For high rotation rates the combined effects prevent the formation of the small negative zonal flow and produce completely positive (but weak) zonal flow at the top level.

f. Stability of the solutions

For the above solutions to exist physically, they must be stable to disturbances in the ϕ-direction. The study of non-rotating, planar Bénard convection indicates that for the Rayleigh numbers of the above solutions that two-dimensional rolls are the preferred mode. However, the analysis of Busse (1970) suggests that in the rotating shallow-shell system, three-dimensional cells are the preferred convective mode irrespective of Rayleigh number. This latter analysis is limited to small Taylor numbers. [The analyses of Roberts (1968) and Gilman (1972) for large Taylor numbers are not applicable to the shallow-shell system.] To resolve the ambiguity between the Cartesian and Busse results we carried out three-dimensional integrations, discussed below, which show that the Busse results only hold for very small rotation effects and do not apply to our flows where rotation effects are large and sufficiently dominant to suppress convection in some regions.

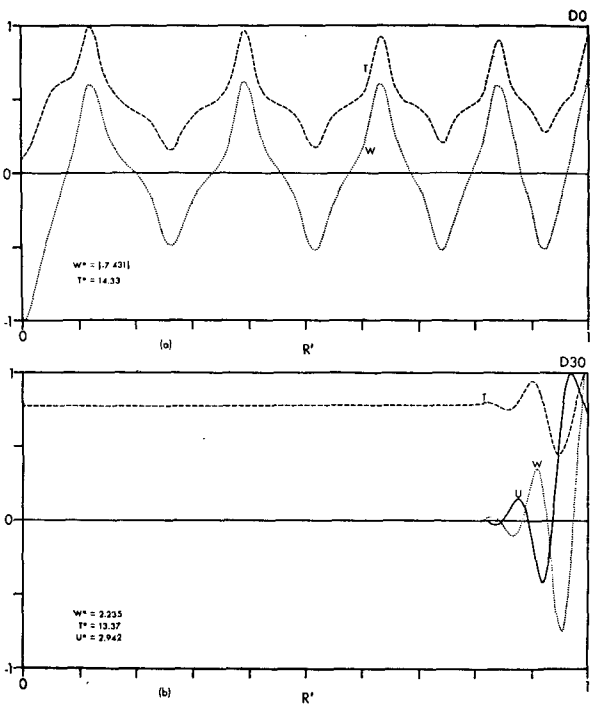

FIG. 5. Cases DO and D30 latitudinal profiles. Legend and units as in Fig. 3.

It would seem that we could obtain a rough estimate of the validity of Busse's theory and of the axisymmetric theory by evaluating the barotropic instability criterion for the solutions. This instability can arise because the rotation produces shears between the positive and negative zonal jets. The criterion for the instability to occur is that the relative vorticity parameter,[8] $B=u_{\theta\theta}/(2\Omega a \sin\theta)$, pass through the value 1.0 (Kuo, 1949). The criterion B was calculated as a function of θ for the upper surface zonal velocity of all solutions, as shown in Fig. 7. The maximum values of B are listed in Table 1. These values suggest that the lower the rotation rate, the higher the value of B and the greater the possibility of instability. The case A2 represents a marginal state for the set A flows as cases with $\Omega>0.2$ are barotropically stable whereas those with $0<\Omega<0.2$ are unstable. These results suggest that axisymmetric convection cannot exist poleward of 45° for the set A flows (the range of A2) and that axisymmetric convection is essentially an equatorial phenomenon.

However, the barotropic instability criterion is derived for a frictionless fluid so that values of B may

[8] An approximate form for spherical geometry.

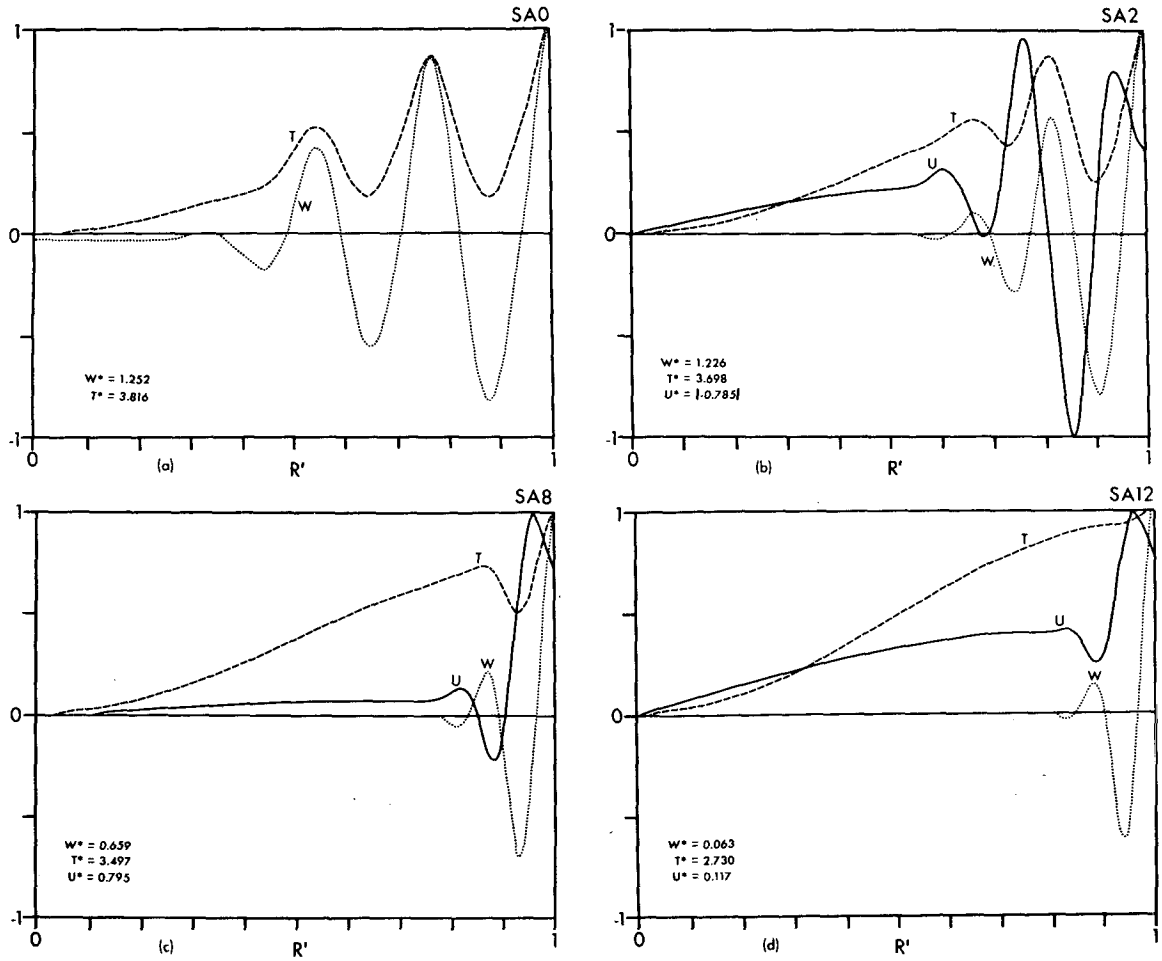

FIG. 6. Set SA latitudinal profiles. Legend and units as in Fig. 3.

not be an accurate predictor of instability in a real fluid. To resolve the issue more definitively, we test the stability of some key flows by three-dimensional (3-D) integration. To make the test, the axisymmetric solution is significantly disturbed by adding a random (in θ, ϕ, z) distribution with an amplitude of 0.2 ΔT to the temperature field. Then the 3-D integration is continued for a length of time comparable to the time scale for the formation of the steady axisymmetric solution.

The 3-D calculations indicate that the axisymmetric flows A2 and A1 are stable so there is no doubt that such flows can exist physically. However, we have also found stable 3-D solutions at the same parameter values. The solutions are essentially combinations of the positive and negative axisymmetric solutions. This degeneracy of uniqueness—a characteristic of Bénard convection—greatly complicates the question of stability. For the flow A1, the B parameter reaches a value of 18 near the pole and has a value of 2 over most of the sphere, yet the flow remains stable. We must therefore conclude that in these flows the friction is sufficiently large to prevent the growth of barotropic instability and that the parameter B is not a good guide to laboratory-scale flow stability.

To try to find a flow to which Busse's analysis might apply, we have made 3-D calculations with very small values of Ω starting from initial conditions of no motion. Since these motions do seem to be 3-D, we must therefore conclude that Busse's analysis is valid only for very small Taylor numbers and thus does not apply to the flows considered in this paper. The axisymmetric flows of this paper are geostrophic with low Rossby numbers, whereas the Busse flows have zonal motions that are predominantly inertially produced.

g. *Conclusions from laboratory-scale calculations*

The flows depicted in the above solutions, although simple, possess in some cases common characteristics with the Jupiter circulations. Related features are 1) the axisymmetric banded pattern (e.g., Fig. 2), 2) the same differential rotation of the $w>0$ zones and $w<0$ belts, and 3) a jet-like tropical zonal flow in high-rotation cases. The existence of stable axisymmetric

convection only at higher rotation rates, and then only equatorward, is consistent with the observed uniformity of the planetary polar regions.

Apart from certain atmospheric similarities, the following general results emerge:

1) A tropical "jet" can be produced by a stable axisymmetric flow [Fig. 3(ii)c].

2) Axisymmetric flow is favored in higher rotation cases and their associated equatorward confined regions of activity.

3) The variation of $\Omega\cos\theta$ in the Taylor number aligns the rolls parallel to the equator by producing higher Taylor numbers and then greater convection suppression at higher latitudes.

4) The range of convective activity is determined by $R/Ta^{\frac{1}{2}}$ and the maximum amplitude of the convection by R.

4. Basic planetary-scale convection

There is, of course, a great deal of difference between the flow of the simple hypothetical laboratory cases of Section 3 and the actual Jovian circulations. However, the similarities lead us to inquire whether such convective modes can organize themselves and be reconstructed on a planetary scale and whether the required formulation is a reasonable representation of the real turbulent process. These questions will be considered in this and the following two sections.

a. Transversely-isotropic convective instability: Linear theory

To produce flows like A2 on a planetary scale the fluid has to form convective cells whose horizontal length scale is much greater than their vertical length scale. If the zone-belt structure is an indication of large convection cells, then the cell aspect ratio γ is of the order of 200 when the depth is 100 km. The atmosphere has an overall aspect ratio of $O(10^3)$.

Although classical convection theory for laminar motion and the solutions in Section 3 predict a cell aspect ratio ≈ 3, it can be shown that the aspect ratio can be altered when the fluid has non-isotropic diffusivities. Linearized perturbation analysis for the non-isotropic convection problem (Williams, 1972) gives that the cell aspect ratio is $\gamma = 2m^{\frac{1}{4}}$, where $\nu_H = m\nu_V$ and $\kappa_H = m\kappa_V$ with m being the relative mixing factor. (This result for free slip boundaries in a non-rotating Cartesian system indicates the general behavior.) The associated critical Rayleigh number is $R_c = 4\pi^4 m$.

In a shallow atmosphere the horizontal length scale is much larger than the vertical, and it is customary to invoke eddy diffusivities such that $\nu_H \gg \nu_V$, i.e., m is large. Such diffusivities could therefore produce the desired elongated cells. However, it has not been possible to establish whether such diffusivities are a valid representation of the multi-scale mixing of a turbulent convective atmosphere. This problem of turbulence theory will be discussed later (Section 6), and for present purposes we invoke the validity of the eddy diffusivities and apply formally the system of Eqs. (7)–(11) to Jupiter-scale calculations.

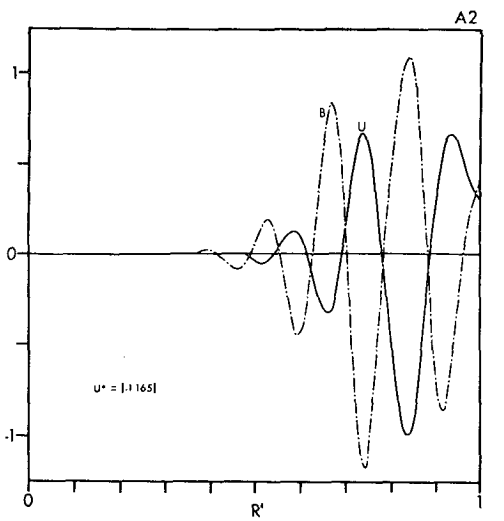

FIG. 7. Case A2: Latitudinal profiles of normalized zonal velocity ($u/u^*\times 10^2$) and barotropic instability criterion $B = u_{\theta\theta}/(2\Omega a \sin\theta)$ at $z = d$.

b. Parameter selection routine

In designing the calculations, values must be chosen for the parameters

$$a,\ g,\ \Omega,\ T_0,\ \beta,\ d,\ \Delta T,\ \nu_H,\ \nu_V,\ \kappa_H,\ \kappa_V.$$

For Jupiter, $a = 7\times 10^4$ km, $g = 2.6\times 10^{-2}$ km sec^{-2}, and $\Omega = 1.76\times 10^{-4}$ sec^{-1} are well-established values. (The unit of length of the parameters and variables is taken in the calculations to be the kilometer because of the large values involved). The effective planetary temperature is estimated to be 130K, and such a value is taken for T_0 to give $\beta = T_0^{-1} = 8\times 10^{-3}$ (°K)$^{-1}$ as the expansion coefficient.

Since the atmospheric depth d remains an unknown quantity, solutions will be obtained with values of d within the speculated range $d = 20$, 50, 100, 500, 1000 and 5000 km. To make these calculations, which include cases with relatively deep atmospheres, the asterisk terms in (1)–(3) are retained and the full axisymmetric equations integrated each time.

For an assumed d, values of ΔT, ν_H, ν_V, κ_H, κ_V must then be selected. There are no observational estimates for these parameters so their values must be deduced by *indirect* inference using our theoretical framework.

Consider the quantitative data items that are available:

1) The range of maximum activity spans $\theta = 70°$–$90°$. This provides an approximate mean latitude measure θ_E for this region given by $\cos^{-1} 0.1$.

2) The equatorial progression and its adjacent regression have a width of $L_E \approx 25{,}000$ km.

TABLE 2. Cases computed for basic planetary convection. Letters A, B, C, etc., denote increasing fluid depth. Calculations use Jovian geometric configuration, i.e., $a=7\times10^4$ km, $\Omega=1.76\times10^{-4}$ sec^{-1}, $g=2.6\times10^{-2}$ km sec^{-2}, $\beta=8\times10^{-3}$ (°C)$^{-1}$. Ta$=7.7\times10^5$ and $d_E=0.15$ are constant. Cases PC and PE are solved for positive and negative flow. Ro$=u_{max}/(2\Omega L_2)$, where $L_2=a\pi/4$. The domain of integration is 45°−90° except for PF which is 0°−90°. Values with daggers are those given by solutions.

Case	d (km)	ΔT (°K)	ν_V, κ_V (km^2 sec^{-1})	m	R	Nu†	u_{max}† (km sec^{-1})	Ro†	B_{max}†	Resolution θ, z
PA	20	150	1.6×10^{-4}	3×10^6	9.8×10^9	1.17	0.108	5.6×10^{-3}	0.98	40, 32
PB	50	60	1.0×10^{-3}	5×10^5	1.6×10^9	1.13	0.098	5.0×10^{-3}	0.79	60, 32
PC +	100	30	4.0×10^{-3}	1.25×10^5	3.9×10^8	1.14	0.091	5.0×10^{-3}	0.81	40, 32
PC −						1.19	−0.124	6.4×10^{-3}	0.59	
PD	500	6	0.1	5×10^3	1.6×10^7	1.12	0.082	4.2×10^{-3}	0.62	40, 32
PE +	1000	3.5	0.4	1.25×10^3	4.6×10^6	1.16	0.099	5.1×10^{-3}	0.83	40, 32
PE −						1.14	−0.133	6.9×10^{-3}	0.74	
PF	5000	3	10.0	50	7.8×10^5	1.28	−0.367	1.9×10^{-3}	4.40	80, 32

3) The tropical jet has an amplitude of 0.1 km sec^{-1}.

4) The variation of u with latitude at cloud level has a definitive profile (Chapman, 1969).

The above data can be used to estimate parameter values if the results of linear anisotropic convective instability theory are invoked. Since observational evidence is insufficiently sensitive to infer the Prandtl number, $\sigma=\nu/\kappa$, values are therefore taken to be unity, i.e., $\nu_H=\kappa_H=m\nu_V$. The linear theory predicts that for high Taylor numbers the cell wavelength-to-depth aspect ratio is given by $\gamma=2\pi m^{\frac{1}{2}}T_E^{-\frac{1}{4}}$, where $T_E=\mathrm{Ta}\cos^2\theta_E$ defines a local Taylor number on the

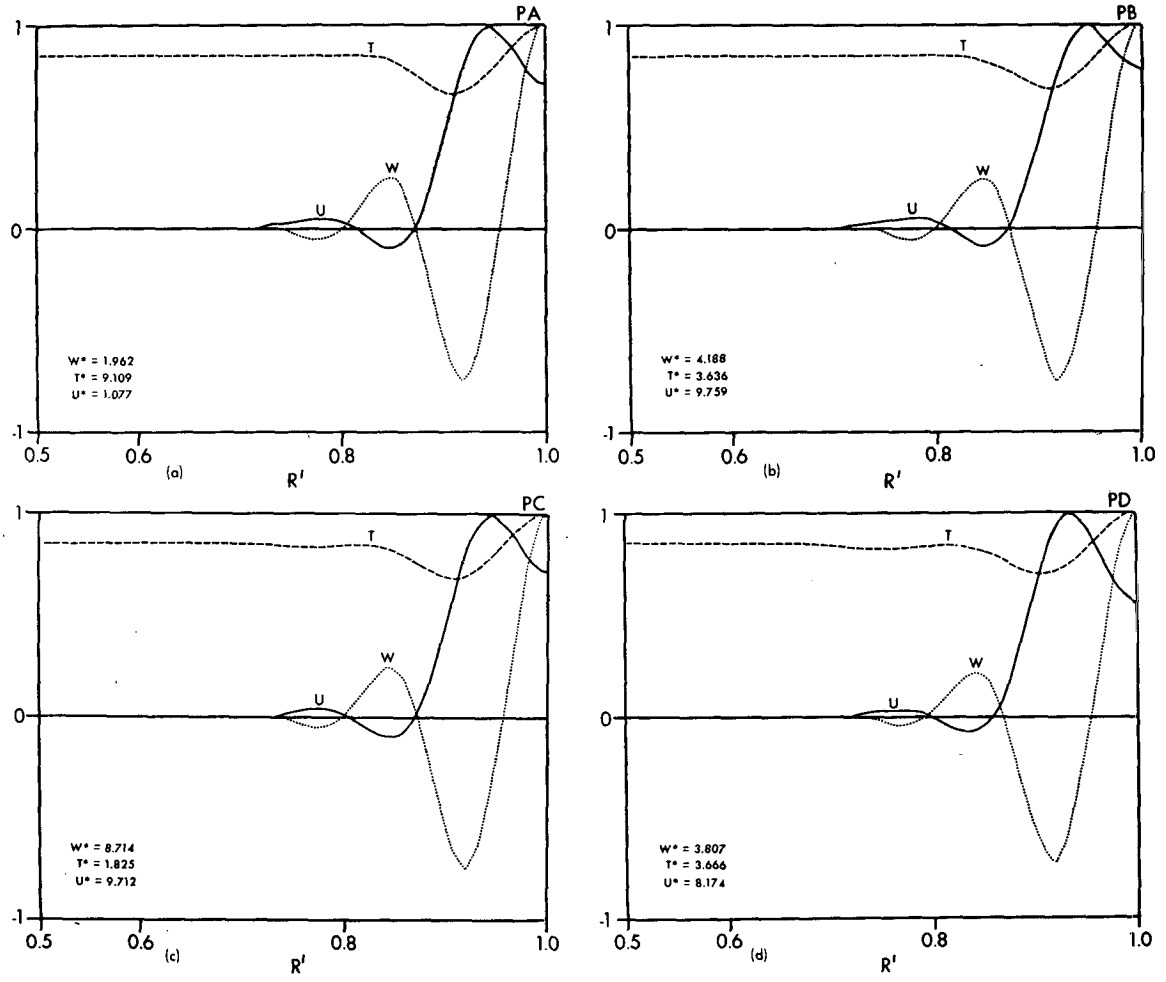

FIG. 8. Set P planetary-scale cases: latitudinal profiles of u/u^* [km sec^{-1}] at $z=d$ and w/w^* [km sec^{-1}], T/T^* [°C] at $z=d/2$. Units of w^*, T^*, u^*, respectively, are for Fig. 8(i): a. 10^{-4}, 10, 10^{-1}; b. 10^{-4}, 10,10^{-2}; c. 10^{-4}, 10, 10^{-2}; d. 10^{-3}, 1, 10^{-2}; and for Fig. 8(ii): a. 10^{-3}, 1, 10^{-2}; b. 10^{-3}, 1, 10^{-1}; c. 10^{-2}, 1, 10^{-1}.

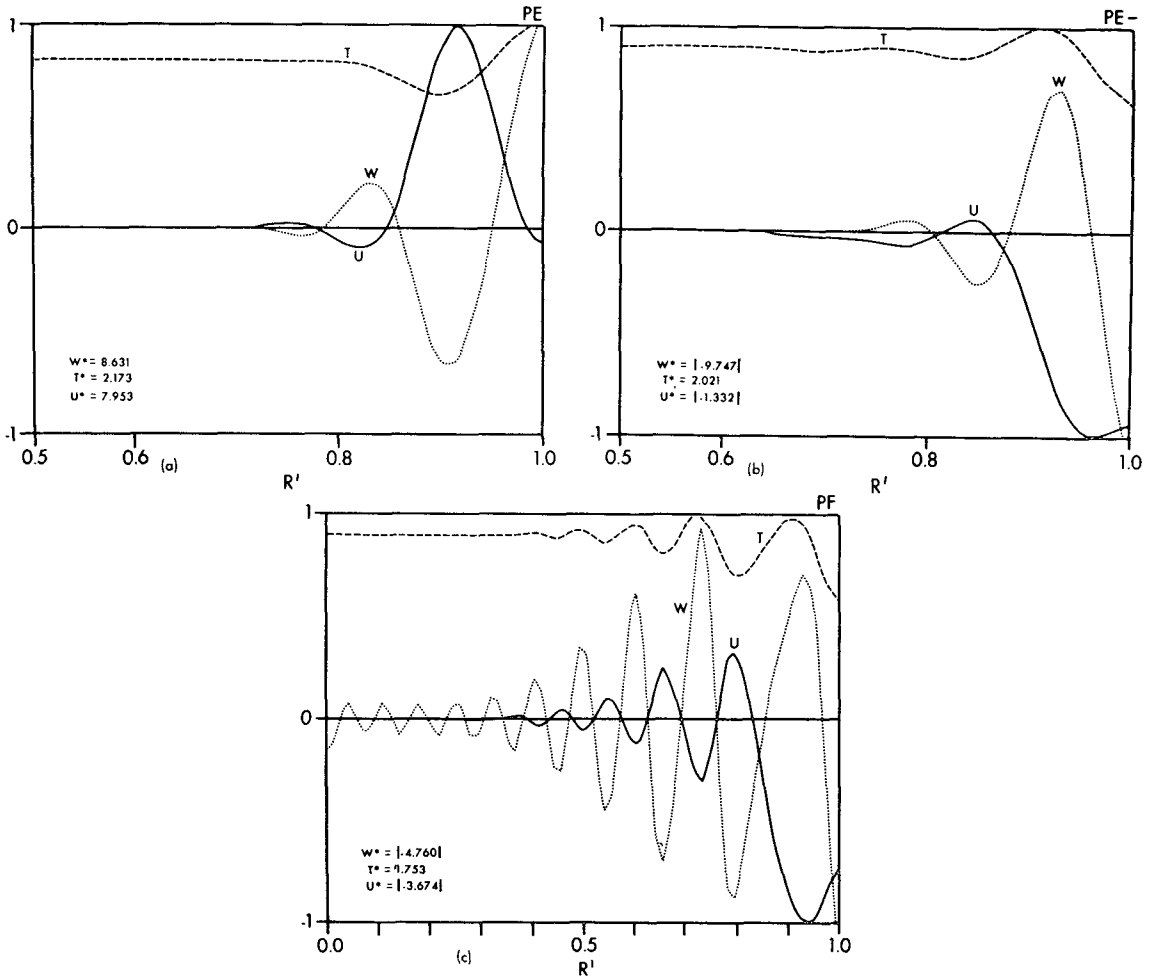

FIG. 8. (*continued*).

sphere. If L_E/d is a measure of the planetary γ, then we have

$$m=\frac{T_E^{\frac{1}{2}}}{4\pi^2}\left(\frac{L_E}{d}\right)^2, \tag{15}$$

so that m is known in terms of ν_V. Data items 1) and 2) from above are required in (15).

Furthermore, the limited range of convective activity indicates that the Rayleigh number for the large-scale mean motion is close to the critical value for the given Taylor number as the flow becomes subcritical at the end of the activity range. From linear theory, $R_c=2\pi^2 m T_E^{\frac{1}{2}}$ for a free-free boundary system. For a rigid-free boundary system we assume that the situation resembles the classical Bénard one and introduce a factor of 2 so that $R_c=4\pi^2 m T_E^{\frac{1}{2}}$. Substituting R and Ta into this R_c equation gives

$$d\Delta T=\frac{4\Omega^2}{\beta g}L_E^2\cos^2\theta_E, \tag{16}$$

with the unknown ν_V canceling out. Data items 1) and 2) and the $\sigma=1$ assumption also enter (16) and for an assumed d provide an estimate for ΔT. Eq. (16) also indicates that $d\Delta T$ is a constant, a result also suggested by Stone (1967) and Ingersoll and Cuzzi (1969) but for a completely different reason (namely the thermal wind balance) and for $a\Delta_H T$ rather than for $a\Delta_V T$ as in this case.

The above argument indicates that for a given depth there is but one free parameter, ν_V, within the observational and theoretical framework. However, data items 3) and 4) have not yet been used. Although these data cannot provide a direct estimate of ν_V, item 3) can be used *a posteriori* to improve an initial guess. A first approximation to ν_V can be taken to be such that the grid Reynolds number $\mathrm{Re}=w\Delta z/\nu_V$ is of the order unity, and in practice item 3) is needed to give a value of w.

The routine for estimating parameter values provides only a first approximation to their values because the quantity θ_E is ill-defined and the procedure is based on

a limited linear theory. However, the routine does form a good first step from which to iterate the parameters toward values giving more realistic solutions.

The observational item 4), on the shape of the u profile, is not used in determining parameter values and so remains as the main test of the solutions. If alternative observations had been available, the parameter selection procedure would have followed a different logic, e.g., if ΔT is known, Eq. (16) gives an estimate for d.

c. *Parameter values*

Solutions were obtained for the range of parameter values listed in Table 2. These values were chosen to be related to parameters of a reference case PB. This case was taken to be the basic one as its depth, 50 km, seemed to represent the most realistic estimate of the planetary-scale height.

The routine of Section 4b provided the parameter values for PB. To estimate ν_V from the grid Reynolds number $\mathrm{Re}=w\Delta z/\nu_V\approx 1$, w is taken from the conservation equation to be $w\approx ud/L_E$ so that $\nu_V\approx ud\Delta z L_E^{-1}$ $\approx 10^{-3}$ km^2 sec^{-1}. Then with a value of $\nu_{V_0}=1\times10^{-3}$ km^2 sec^{-1}, we obtain from Eqs. (15) and (16) $m\approx 5\times10^5$ and $\Delta T\approx 60$K. Calculations made with parameter values so estimated, provide a realistic zonal velocity maximum of 0.1 km sec^{-1} and are maintained as the final choice for case PB. No iteration of parameters is necessary but this is fortuitous in view of the ill-defined θ_E quantity.

The parameter values for the other cases in Table 1 are derived from the PB values by keeping $d\Delta T$ and Ta constant. This gives ν_V and ΔT values in terms of the PB values. The resulting solutions then all have a maximum $u\approx 0.1$ km sec^{-1} because of (16) and a thermal wind balance. One exception to this was the case PF where a higher temperature than that predicted by $d\Delta T=$constant is necessary to make the flow critical. The difference is due to the fact that at the depth of case PF the flow exhibits a different convective mode, that discussed by Busse (1970) and Gilman (1972), for which the linear theory no longer applies.

d. *Discussion of solution set* P

The solutions for the cases of Table 2 are shown in Figs. 8–11. The flows of PA, PB, PC, PD are similar in most respects [Fig. 8(i)], so that only the reference case PB requires detailed attention. Its contours are given in Fig. 9. Case PD with its smaller u value at the equator is indicative of a transition to the PE flow type that occurs as the depth and the influence of the equatorial region through the $\Omega\sin\theta$ terms increases. At a depth of 5000 km the flow PF enters a completely different convective regime, one that is associated with a deep atmosphere [Fig. 8(ii)c].

The PE contours (Fig. 10) display a slight vertical sloping, a characteristic which is more apparent in the deep convection flow PF (Fig. 11). The positive and negative solutions PE, PE− indicate that a strong

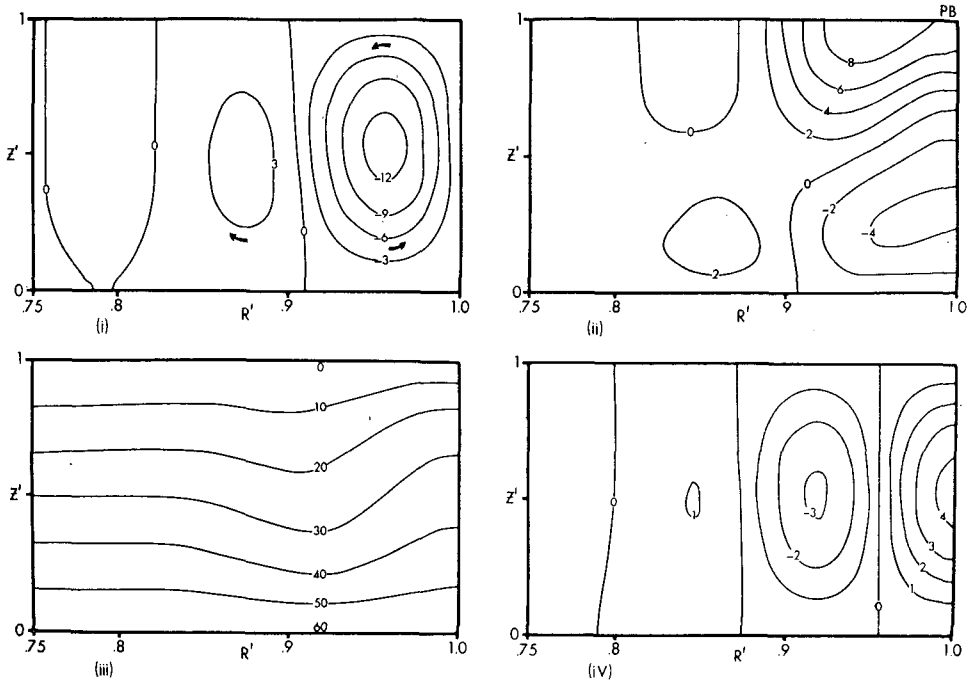

FIG. 9. Case PB: contours in equatorial region of (i) $\psi\times10^1$ [km^2 sec^{-1}]; (ii) $u\times10^2$ [km sec^{-1}]; (iii) T [°C]; (iv) $w\times10^4$ [km sec^{-1}].

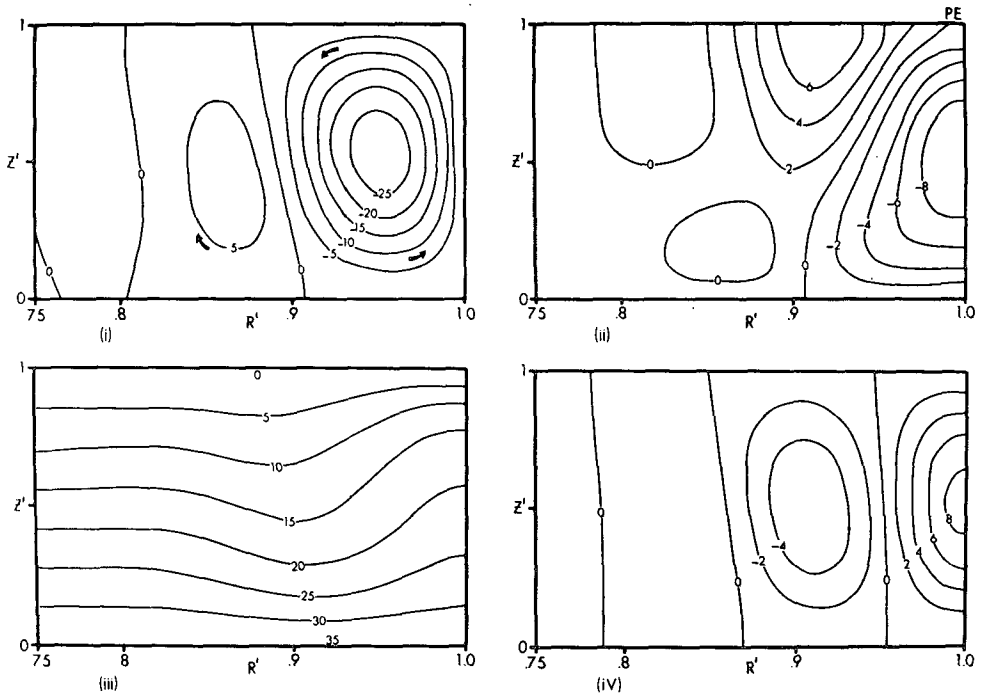

FIG. 10. Case PE: contours in equatorial region of (i) ψ [km^2 sec^{-1}]; (ii) $u\times10^2$ [km sec^{-1}]; (iii) ($T\times10$ [°C]; (iv) $w\times10^3$ [km sec^{-1}].

positive equatorial zonal flow cannot be produced for this atmospheric depth.

For the deepest atmosphere (PF) only one solution exists and it has negative equator values of u and w [Figs. 8(ii)c and 11]. The cellular rolls tend to slope parallel to the rotation axis in the equatorial region. Of the P set, only the flow PF could be barotropically unstable ($B\approx4.0$), and the enforced axisymmetry could explain the singular difficulties encountered in obtaining a steady solution for this case.

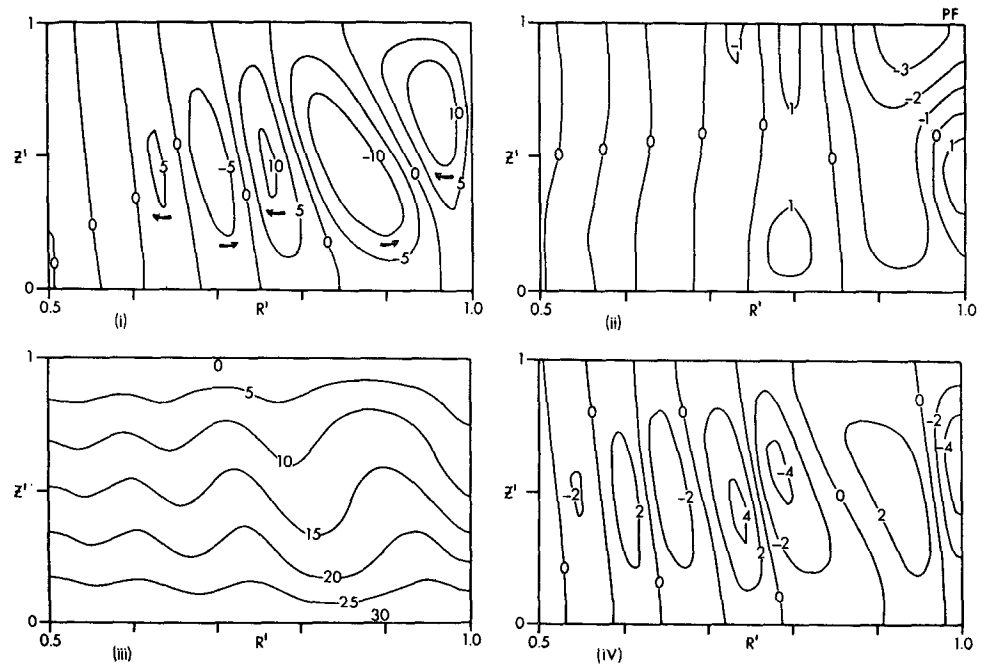

FIG. 11. Case PF: (i) $\psi\times10^{-1}$ [km^2 sec^{-1}]; (ii) $u\times10$ [km sec^{-1}]; (iii) $T\times10$ [°C]; (iv) $w\times10^2$ [km sec^{-1}].

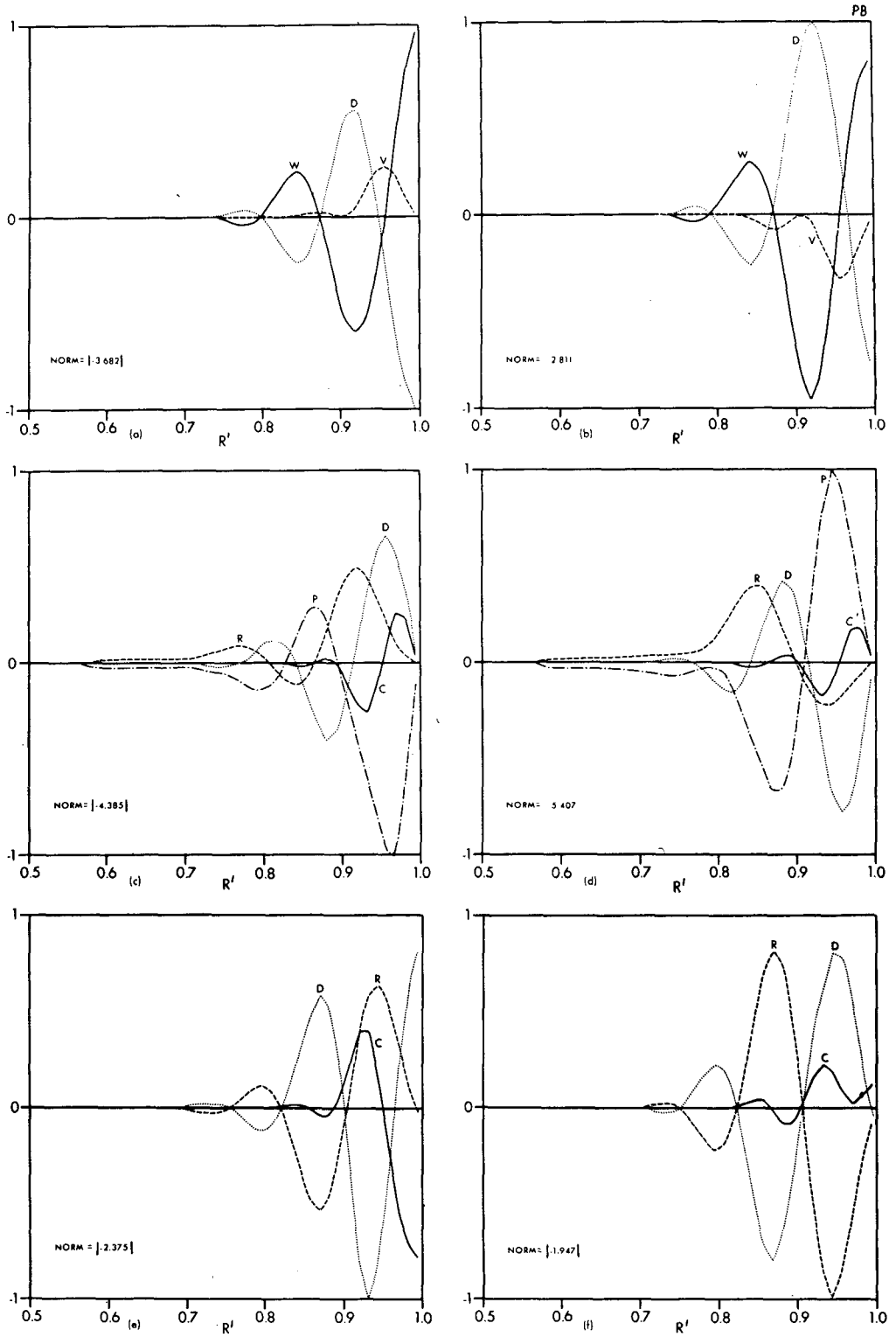

FIG. 12. Latitudinal distributions of representative components of the prediction case PB. Equations for prediction equations are for: (a) T at $z'=\frac{3}{4}$, (b) T at $z'=\frac{1}{4}$, (c) v at $z'=\frac{3}{4}$, (d) v at $z'=\frac{1}{4}$, (e) u at $z'=\frac{3}{4}$, (f) u at $z'=\frac{1}{4}$. Components are (a), (b): $W\equiv -wT_z$, $V\equiv -vT_\theta/a$, $D\equiv F_T$ [Eq. (11)]; (c), (d): $\mathrm{R}\equiv[2\Omega+(u/a\sin\theta)]\,u\cos\theta-(vw/a)$, $P\equiv -p_\theta/a$, $D\equiv F_v$ [Eq. (8)], $C\equiv -\mathbf{v}\cdot\nabla v$; (e), (f): $\mathrm{R}\equiv -[2\Omega+(u/a\sin\theta)]\,(v\cos\theta+w\sin\theta)$, $D\equiv F_u$ [Eq. (7)], $C\equiv -\mathbf{v}\cdot\nabla u$. Terms are normalized with respect to the extreme component value. Units are (a), (b): 10^{-4}C sec^{-1}; (c), (d), (e), (f): 10^{-6} km sec^{-2}.

We conclude that for these solutions to be relevant to Jupiter the active atmosphere must be relatively shallow, i.e., <500 km. In the remaining calculations, $d=50$ km is taken as a representative estimate. However, the similarity of the solutions for $d=20-500$ km means that the results can be quantitatively modified by changing d within this range.

e. *Dynamics of the reference case* PB

Comparison of the zonal velocity profile of case PB with that of Jupiter in Fig. 13(b), curve A, reveals similar jet widths and amplitudes. The PB flow consists of an upper level positive zonal flow and lower level negative zonal flow in $R'=0.9$–1.0 [Fig. 9(ii)]. The flow is barotropically stable. The meridional flow consists mainly of a single large direct cell in $R'=0.9$–1.0 and of weaker cells to the north of it.

The dynamical maintenance of the PB flow can be gauged from the balance of the representative component terms of the basic equations (Fig. 12). The w_t components are omitted because the flow is in an approximately hydrostatic balance. The components of the T_t equation simply reflect the basic ψ, T patterns and the balance of linear theory. The v_t components show that the meridional motion produces a pressure gradient p_θ/a which maintains the cell against dissipation and Coriolis deflection. The u_t components demonstrate that the jet maximum at $R'=0.95$ is produced by Coriolis deflection of the meridional flow. This jet maximum is held in equilibrium by a diffusion which is mostly transferring momentum laterally through the term $\nu_H u_{\theta\theta}/a^2$ to maintain the zonal velocity at the equator.

The overall flow arrangement indicated by the balances is one in which a large convective cell is set up in $R'=0.9$–1.0. Coriolis forces then deflect this cell to produce a zonal velocity maximum at $R'=0.93$ at the upper level and a zonal velocity minimum at the base. Lateral mixing then acts to drag the fluid at the equator along with the jet just poleward of it. This produces a fairly flat u profile in $R'=0.9$–1.0.

The related angular momentum balance is straightforward. The main cell transports angular momentum upward from the source in the negative zonal flow at the base $R'=0.9$–1.0 region (Fig. 9) to the upper level jet at the base $R'=0.9$–1.0 region (Fig. 9) to the upper level jet at $R'=0.93$. This source maintains the maximum u against diffusive transfer to the equator and against transfer to the sink region in the positive zonal velocity flow at the base $R'=0.8$–0.9 region. The balancing of source and sink at the base provide global equilibrium.

The damped sinusoidal variation of the various component terms in Fig. 12 suggest that the simple instability mode of linear theory determines the shape of the steady-state flow pattern.

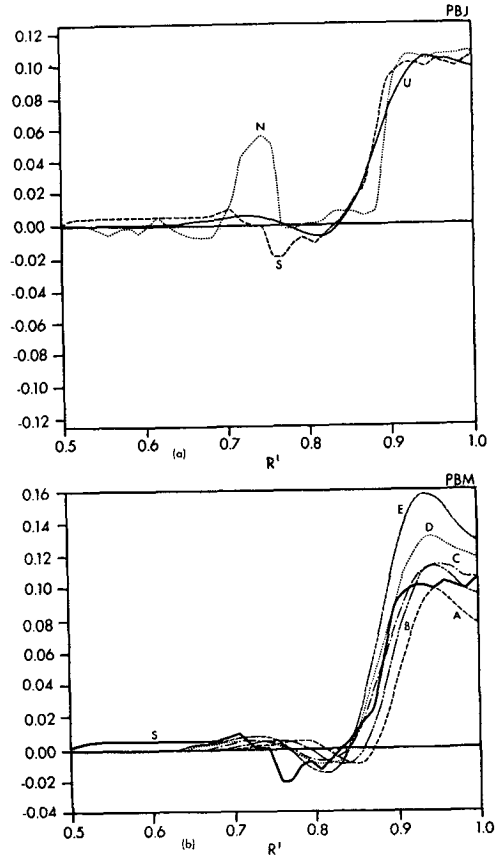

FIG. 13a. Comparison of the best zonal velocity latitudinal profile at $z=d$ produced by the linear viscosity model, case PBJ, and the mean observed profiles, after Chapman (1969). Letters denote U (solution), N (Northern Hemisphere data) S (Southern Hemisphere data). Units are km sec^{-1}. FIG. 13b. Comparison of the zonal velocity latitudinal profiles at $z=d$ produced by the set of multiple solution PBM with the observed Southern Hemisphere profile, after Chapman (1969). Units are km sec^{-1}.

5. Specific planetary-scale solutions

Having seen that flows with some Jovian characteristics can be produced by the linear eddy viscosity model, we now consider how close a solution to the observed flow can be obtained with this model and how sensitive the solutions are to the choice of parameter values and boundary conditions.

a. *Comparative solutions for Jupiter*

The observed u profiles have significant hemispheric differences as shown in Fig. 13a. As the comparison in this section involves mainly the tropical jet, either hemispheric profile is appropriate but the southern one is chosen because of its simpler form (Fig. 13b).

The jet of the reference case PB (≡PBM.A) is deficient in its width and shape compared to the observed, having a marked decline from its peak at $R'=0.93$ to the equator (Fig. 13b). Eq. (15) suggests that a wider jet can be obtained by increasing the rela-

TABLE 3. Specific planetary scale cases, where G indicates global domain, S the presence of secondary heating, M the multiple cases changing only ΔT and m, and J refers to the case closest to Jupiter. All cases take Jovian geometry as $a=7\times10^4$ km, $d=50$ km, $\Omega=1.76\times10^{-4}$ sec^{-1}, $g=2.6\times10^{-2}$ km sec^{-2}, $\beta=8\times10^{-3}$ (°K). Constant parameter values are $\nu_V=1\times10^{-3}$ km^2 sec^{-1}, Ta$=7.7\times10^5$, $d_E=0.15$. The function $f(\theta)=0$ except for $80°<\theta<100°$ where $f(\theta)=\sin^2 9\theta$.

Case	ΔT (°K)	m	R	Nu	Ro	u_{max} (km sec^{-1})	B	θ range	Resolution θ, z	Comments
PBM.A	60	5×10^5	1.6×10^9	1.16	5.0×10^{-3}	0.10	0.8	45°– 90°	40, 22	Parameter spread about Jupiter profile
PBM.B	90	7×10^5	2.3×10^9	1.13	5.8×10^{-3}	0.11	0.7	45°– 90°	40, 22	
PBM.C	135	10^6	3.5×10^9	1.09	5.8×10^{-3}	0.11	0.5	45°– 90°	40, 22	
PBM.D	140	10^6	3.6×10^9	1.13	6.8×10^{-3}	0.13	0.6	45°– 90°	40, 22	
PBM.E	155	10^6	3.9×10^9	1.19	8.1×10^{-3}	0.16	0.8	45°– 90°	40, 22	
PBJ	133	10^6	3.5×10^9	1.07	5.4×10^{-3}	0.10	0.5	45°– 90°	40, 22	Case closest to Jupiter
PBG1	60	5×10^5	1.6×10^9	1.14	5.2×10^{-3}	0.10	0.8	45°–135°	80, 22	Global symmetric mode
PBG2	60	5×10^5	1.6×10^9	1.34	5.2×10^{-3}	−0.10	1.2	45°–135°	80, 22	Global anti-symmetric mode
PBS1	60†	5×10^5	1.6×10^9 (max)	—	6.2×10^{-3}	0.12	1.5	45°–135°	80, 22	† Base $T=\Delta T f(\theta)$
PBS2	60‡	5×10^5	1.6–2.3 $\times10^9$	—	9.5×10^{-3}	0.18	1.3	45°–135°	80, 22	‡ Base $T=\Delta T+\Delta T f(\theta)/2$ (symmetric mode)
PBS3	60¶	5×10^5	1.6–3.1 $\times10^9$	—	1.4×10^{-2}	0.27	2.0	45°–135°	80, 22	¶ Base $T=\Delta T+\Delta T f(\theta)$ (anti-symmetric mode)

tive mixing factor m. The results of four calculations with increasing m values, as listed in Table 3, are shown in Fig. 13b; ΔT is also increased to achieve the larger critical Rayleigh number of these cases but other parameters remain constant.

The u profiles show that the jet width is a function of m only with curves C, D, E intersecting the axis at the same point. Comparing these three curves, a constant m indicates that a larger ΔT produces a larger maximum u but also a more peaked profile. Of all these cases only C has a flat jet profile in $R'=0.93$–1.0.

The result that emerges from Fig. 13b is that there is an inter-relationship between the jet width, amplitude and shape. It would not be possible to satisfy these three criteria with two variable parameter values unless this inter-relationship existed, and for this association to be correctly simulated the model has to be realistic. Thus, for example, only when the computed jet has the same width and amplitude as the observed can it also have the same shape. This freedom in the system and the ability of the model to achieve a self-determined shape suggests that the model may well be realistic.

The most realistic solution PBJ (Fig. 13a) coincides with the observed Southern Hemisphere profile to within the limit of observational errors in $R'=0.8$–1.0. The temperature differential of $\Delta T=133$K would be different if d differed and a non-Boussinesq compressible system was used. This uncertainty plus the fact that the Boussinesq temperature corresponds to the atmospheric potential temperature makes quantitative comparisons with the planet impossible.

Despite agreement between the equatorial u distributions, the comparison with Northern Hemisphere data is poor in the $R'=0.5$–0.8 region and the predicted w bands are too weak in that region. This deficiency will be reduced by the model to be discussed in Section 6.

Although the flow PBJ is barotropically stable, a 3-D calculation shows that the convective rolls are unstable and that cells are the preferred mode. This matter is discussed further in Section 7.

b. Global mode selection

The possibility of realizing both positive and negative solutions in a global domain allows either a symmetric or antisymmetric mode to occur. Such modes for the global cases PBG1, PBG2 corresponding to the hemispheric reference case PB are illustrated in Figs. 14–16.

To find out whether the fluid has a preferred mode, calculations were made for multiple R and Ta values in the region of PB values from subcritical to critical flow. Both symmetric and antisymmetric modes exist together initially and although the final solution should depend on which mode has the faster growth rate, the rates seem indistinguishable so that the final flow mode is somewhat arbitrary.

If the growth rates do not select the mode then some other mechanism must, whether it be secondary heating effects or the 3-D aspect of the motion. The barotropic instability condition shows that antisymmetric motion is less stable. The antisymmetric mode also requires a wider latitudinal range for its existence. Although these two points suggest that the antisymmetric mode is less likely to exist, the problem requires further examination.

Observations of Jupiter indicate the presence of a symmetric flow system. However, it is possible that the antisymmetric mode could be activated to give some of the transient features of the atmosphere, e.g., the changing band structure. The full contours of both modes (Figs. 15 and 16) are representative of how much the linear viscosity model can produce. Additional contours have been added for PBG1 to illustrate the

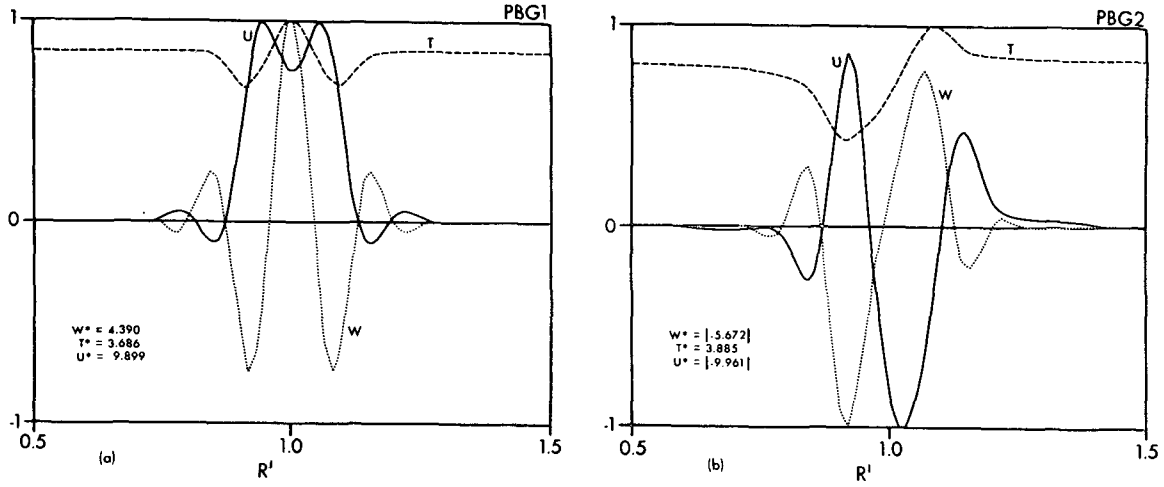

FIG. 14. Latitudinal profiles of normalized basic variables w/w^*, T/T^*, u/u^* for global cases PBG1, PBG2. Equator is at $R' = 1.0$. Normalized variables have units of 10^{-4} km sec^{-1} for w, 10C for T, and 10^{-2} km sec^{-1} for u.

weaker extra-equatorial motions and band structure. The most striking feature of the antisymmetric flow is its large trans-equatorial cell.

c. *Secondary heating effects*

It is possible that Jupiter could have some latitudinal variation in its basic heating field. These variations could be complex, being caused by external (solar) and secondary internal heating mechanisms. To examine crudely the possible dynamical effects of such variations on an unstable atmosphere, three PBS solutions are obtained for which the temperature imposed along the base is of the form $\Delta T + \Delta T f(\theta)$, where $0 < f(\theta) < 1$ is defined in Table 3. The first term represents the primary heating source and the second represents 1) the effect of enhanced solar heating at the equator, although depending on the cloud structure the enhancement might be better applied at e.g. $\theta = 80°$; and 2) the effect of heating anomalies in the planetary interior caused by the extraction by the atmosphere of more heat in the equatorial region. The ΔT term produces the convective mode whereas $\Delta T f(\theta)$ produces Hadley-type flow through the variation $df/d\theta$.

The flow produced by the secondary heating function $\Delta T f(\theta)$ alone has the form of a broad flat jet (solar like) centered over the equator (PBS1, Fig. 17a). The second case (PBS2), with the mixed primary and secondary heating, has a split jet and weak zonal flow at the equator. The absence of any negative zonal flow at $z = d$ in both solutions suggests that secondary heating sources of this type must be uninfluential on the planet.

The case PBS3 was designed to test the dominance of the convective mode. Given an established antisymmetric mode, the symmetric secondary heat source was added to see if it could induce a symmetric mode to take its place. Fig. 17c shows that it could not, even for a comparable heating strength. Similarly, we can expect that antisymmetric secondary heating effects, if they could exist, would not affect the symmetric convective flow. Thus, the basic flow is determined by primary instability characteristics which are dominant and entrenched, once established, and are not susceptible to secondary influences.

6. Planetary-scale thermal convection

In this section we would like to discuss the two main unresolved questions; namely, how we can justify the use of eddy diffusion coefficients in a gross representation of thermal convection on a rotating planet and how should the turbulence be more fully represented so that more realistic models can be developed in a progression toward a simulation of Jupiter's atmosphere. Our discussion will be inconclusive.

a. *Thermal turbulence*

Although thermal turbulence is discussed in many problems on the laboratory, planetary and solar scale, little progress has been made toward a general theory for this phenomenon.

On the laboratory scale, Kraichnan (1962) has provided a reasonable explanation of isotropic thermal turbulence by the use of eddy diffusivities in a mixing-length theory. Experiments on anisotropic thermal turbulence have been made by Deardorff and Willis (1967) who examined the flow between two large horizontal plates with a narrow gap, a system with a horizontal isotropy comparable to that of a shallow atmosphere. These experiments revealed that thermal turbulence in a shallow system is not random but exhibits "cyclic structures" reminiscent of convection cells. Elongated "cells" with aspect ratios up to 15 were observed. This result provides some justification

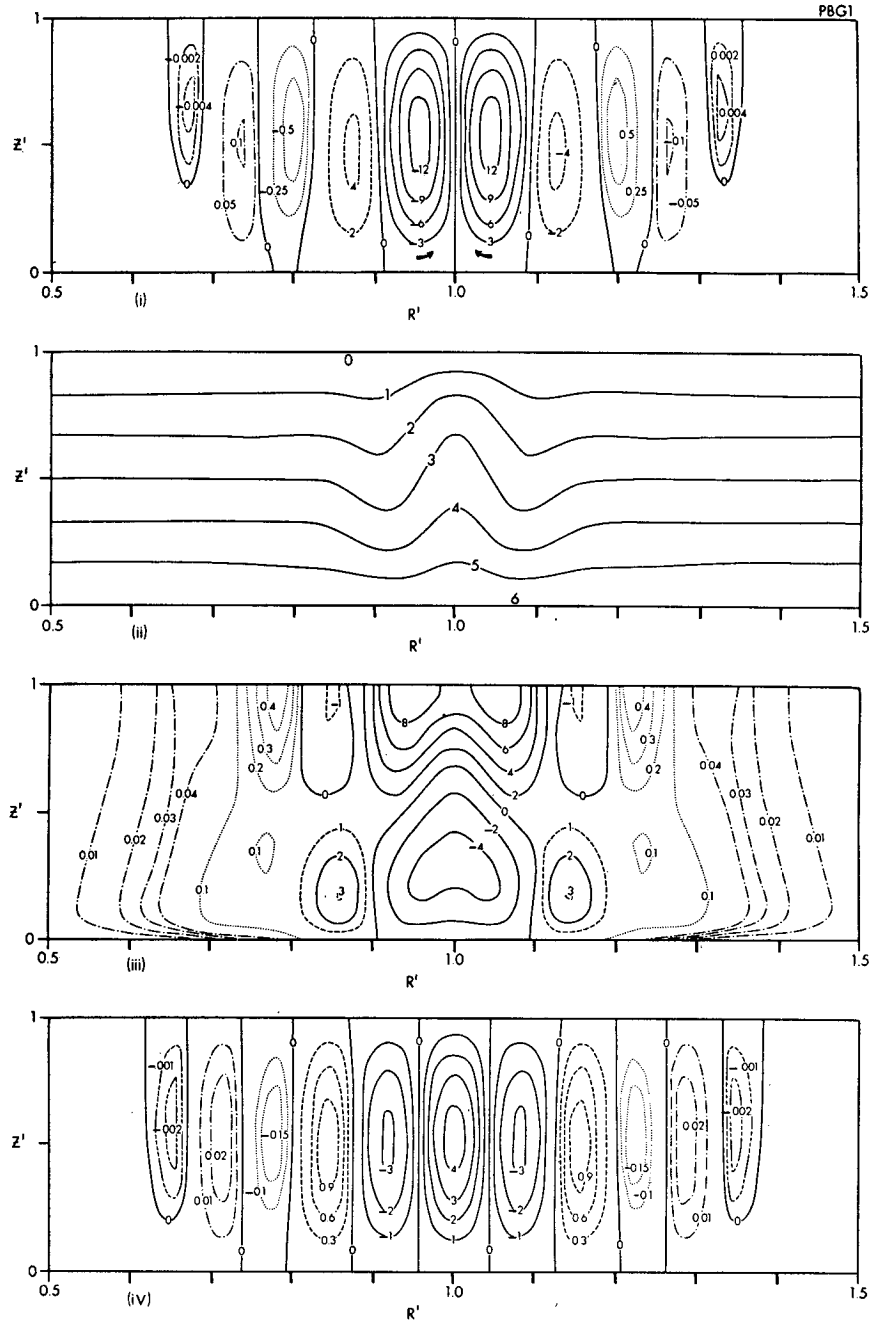

FIG. 15. Contours of the symmetric global mode of PBG1 from 45°–135° latitude: (i) $\psi \times 10$ [km^2 sec^{-1}]; (ii) $T \times 10^{-1}$ [°C]; (iii) $u \times 10^2$ [km sec^{-1}]; (iv) $w \times 10^4$ [km sec^{-1}]. Dashed and dotted contours indicate a smaller contour interval for less active regions.

for the use of eddy viscosities to give the elongated cells in Sections 4 and 5.

The existence of granulation and mean circulations in the solar atmosphere also suggest that at very high Rayleigh numbers thermal turbulence is not random but that an eddy field can be established such that regular cell patterns appear. Eddy diffusivities would seem to be a viable approximation for such a system. The re-establishment of order in the turbulent field would seem to require a very large Rayleigh number and scale variation. That Jovian convection might be a sub-form of stellar convection would be consistent with the pseudo-stellar composition of the planet.

On the planetary scale, thermal turbulence acts as the formulative process in hurricanes and in the inter-tropical convergence zone (ITCZ). In these phenomena,

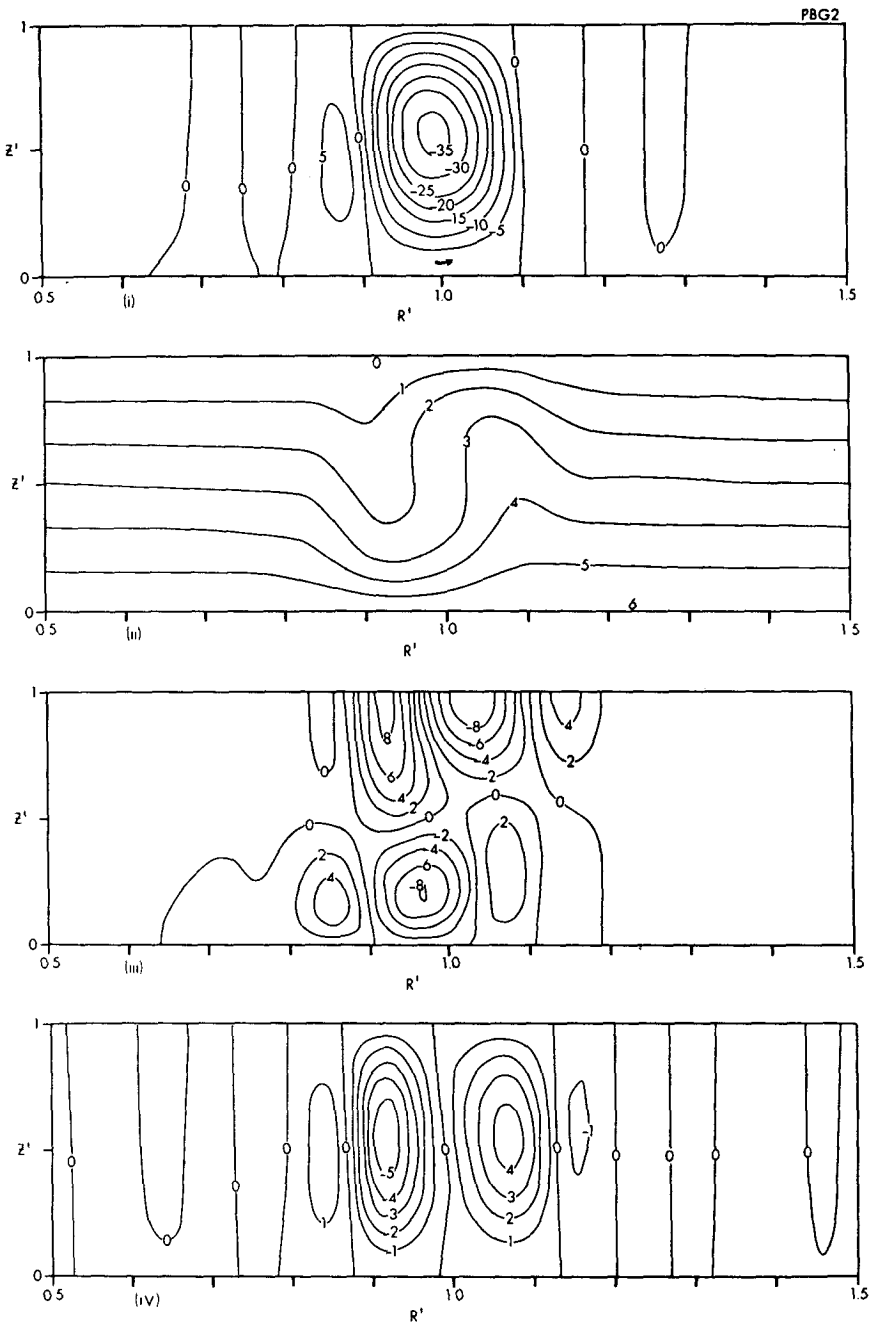

FIG. 16. Contours of the antisymmetric global mode of PBG2 from 45°–135° latitude: (i) $\psi \times 10$ [km^2 sec^{-1}]; (ii) $T \times 10^{-1}$ [°C]; (iii) $u \times 10^2$ [km sec^{-1}]; (iv) $w \times 10^4$ [km sec^{-1}].

the hypothesis that the smaller scale convective elements (cumuli) organize in such a way as to drive the large-scale circulation has been reasonably well established (Ooyama, 1969; Charney, 1970). This scale interaction is made possible by the CISK[9] mechanism which relies on latent heat release for its existence. As this process cannot be assumed to occur on other planets, it is not advisable to extrapolate these ideas to a remote planet. Despite this, it does appear that the ITCZ offers evidence of the existence of a type of convective-scale interaction comparable to that required to explain the Jovian characteristics.

[9] Conditional instability of the second kind (Charney and Eliassen, 1965).

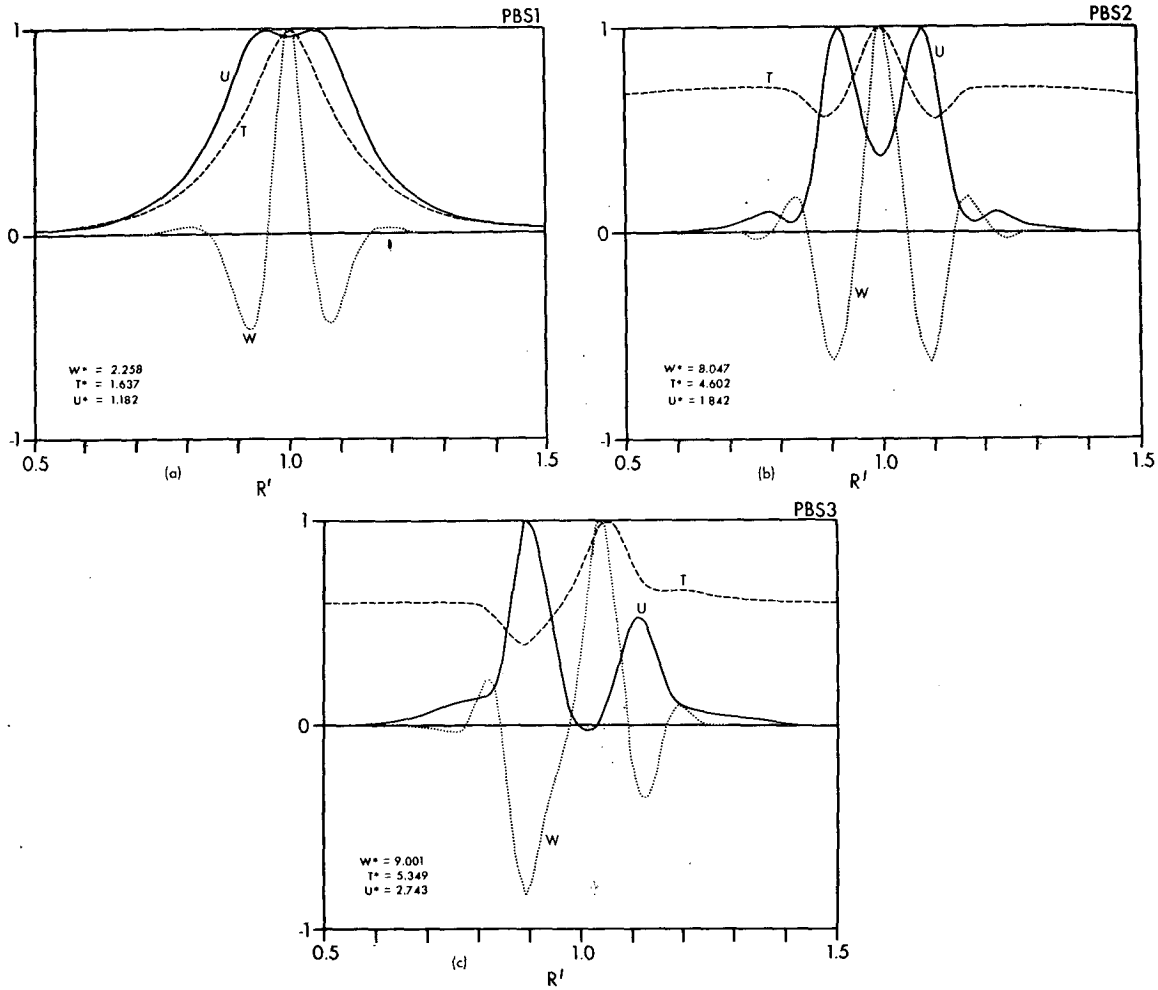

FIG. 17. Latitudinal profiles of normalized variables for three global cases with variable heating at $z=0$: (a) PBS1 has $\Delta T f(\theta)$, (b) PBS2 has $\Delta T+(\Delta T/2)f(\theta)$, (c) PBS3 has an antisymmetric mode with $\Delta T+\Delta T f(\theta)$. Normalized variables have units of 10^{-4} km sec^{-1} for w, 10C for T, 10^{-1} km sec^{-1} for u.

b. Character of Jovian turbulence

If we regard the solution PBJ (Fig. 15) as being a rough guide to the Jovian circulation, then the turbulence on that planet must be considered as being a mixture of shear and thermally driven turbulence. Although there may well exist boundary layers or free layers where one turbulence form predominates, it is not clear which is the dominant process.

The banded structure of Jupiter indicates that the large-scale mean motion is predominantly axisymmetric but that the smaller scale motions within the bands are more three-dimensional. The orderliness of the mean circulation implies that the main energy input to the motion occurs at a medium size (latitudinal) wavenumber≈ 5. In the Earth's extratropical atmosphere, a comparable orderliness in the circulation is produced by the baroclinic instability mechanism releasing potential energy at wavenumber 6 to produce the wavelike structures. However, there could be a significant difference between the ordering modes and the associated turbulence of the Earth and Jupiter if convective instability controls the latter planet. For whereas the baroclinic instability mechanism is independent of the turbulence characteristics, i.e., is quasi-linear, the convective mode depends crucially upon assumptions about the turbulence field. The fact that the magnitude of the eddy coefficients determines the wavelength of the bands (in a shallow atmosphere) leaves the convective instability theory on a less satisfying basis than the baroclinic instability theory of the Earth's extratropics but on a comparable basis to theories for the Earth's tropical circulations. A similar situation occurs or has occurred in studies of the solar circulation, hurricanes, and the tropical circulation in that the baroclinic and convective modes vie in providing an explanation.

The most difficult aspect involved with the convective mode theory for Jupiter is in explaining how the characteristic scale of the large-scale circulation is

determined. It is apparently produced by the collective behavior of the small-scale elements acting through a nonlinear scale-interaction effect which cannot be explained by linear theory. The most familiar example of a scale-interaction phenomenon is that of Bénard convection. In that system the properties of the convection are determined by the molecular properties of the fluid acting in parameterized form through the viscosity and conductivity. Just as on the planetary scale, so in Bénard flow it would seem unlikely intuitively (if we were unaware of the Bénard experiments or Rayleigh's analysis) that the molecular behavior of the fluid would produce not a random transfer but a mean cellular convection. It is less satisfying, however, to have to accept that the Jovian band widths may be determined by the collective action of convection elements that cannot be observed.

c. *Parameterization of Jovian turbulence*

The main problem in treating turbulence on a planetary scale lies in properly representing the interaction between the smaller and larger scales of activity. When the turbulence is thermally driven the problem is even more difficult because the main concern is then with the larger scales of motion and with the cascade of thermal energy so that the simplifying ideas of Kolmogoroff and Heisenberg no longer apply.

The gross austausch coefficients used in Sections 4 and 5 provide the simplest parameterization or closing procedure for turbulent transports. For an unobserved atmosphere it is hard to justify using anything other than the simplest closing procedure in an initial study. The use of these coefficients implies that the main purpose of the small-scale convective elements is to act collectively as an eddy conductivity to transfer thermal energy to the atmosphere. The eddy coefficients embody many (unobservable) physical processes, e.g., convective cloud behavior, that eventually deserve a more meaningful treatment. At this initial stage, however, we have assumed that the eddy coefficients are (indirectly) *measurable* quantities just as are the laminar coefficients. However, we do so with the proviso that such quantities can and should be derivable from the smaller scale properties in the same way that the laminar coefficients can be related to the molecular properties, namely through statistical mechanical equations.

The next level of turbulence theory involves using the mixing-length concept. Such theories give reasonable results in solar turbulence but a complete formulation for thermal or mixed turbulence is unknown. Kraichnan (1964) has pointed out that mixing-length theories are only strictly consistent when the local mixing lengths are much smaller than the length scales related to spatial variations in the mean flow. This condition is not well satisfied in thermal convection so agreement between theory and experiment is unsatisfactory. Despite this, the theoretical approach to solar convection has been predominantly based on mixing-length theory and has met with limited success (Spiegel, 1966, 1971).

The derivations of more specialized parameterizations for convective-scale interacting phenomena have been given for the planetary-scale systems, e.g., by Ooyama (1969) for the hurricane and Charney (1970) for the ITCZ. These formulations are based on a knowledge of the energetics, path lengths, and population characteristics of the observed convective clusters. While this type of theory is vital to meteorology, it does not as yet provide a generalized approach to thermal turbulence problems, as it does not use general Reynolds or Boltzman equations and is completely oriented toward the non-universal condensation process.

The simplest, most general mixing-length parameterization of shear-driven turbulence assumes a closing procedure in which the stresses are taken to be proportional to the local velocity deformation D, i.e.,

$$\bar{\tau}_{ij} \equiv -\overline{u_i' u_j'} + \frac{1}{3}\delta_{ik}\overline{u_k' u_k'} = \frac{K}{2} D, \tag{17}$$

where K is an eddy coefficient tensor (Hinze, 1959, p. 21) and

$$D \equiv \frac{\partial u_i}{\partial x_j} + \frac{\partial u_j}{\partial x_i}. \tag{18}$$

For the numerical simulation of isotropic turbulence, the present practice (Deardorff, 1971) is to take K as being given by

$$K = l^2 |D|, \tag{19}$$

where l corresponds to a mixing length in this generalization of Prandtl's theory. Deardorff (1971) has suggested that (19) also holds for thermal turbulence without modifying l to allow for enhancement of mixing by thermal instability as is generally done in solar convection studies.

For the anisotropic Jovian turbulence the formulation (19) may be inappropriate. However, as it represents the simplest general mixing-length parameterization, we will assume that the free atmosphere is dominated by shearing turbulence so that a parameterization similar to that for turbulence in the Earth's atmosphere (Smagorinsky, 1963) may be used. This allows us to work in terms of known parameters. A separate boundary formulation is not used at this stage as it is preferable initially to let the free atmosphere define its own boundary layers. Thus, for axisymmetric flow the turbulent transports are written (Williams, 1972):

$$F_u = \frac{1}{a^2 \sin^2\theta}[K_H \sin^3\theta (u/\sin\theta)_\theta]_\theta + (K_V u_z)_z, \tag{20}$$

$$F_v=\frac{1}{a^2\sin^2\theta}[K_H\sin^3\theta(v/\sin\theta)_\theta]_\theta+(K_Vv_z)_z, \quad (21)$$

$$F_w=\frac{1}{a^2\sin\theta}(K_V\sin\theta w_\theta)_\theta+(K_Vw_z)_z, \quad (22)$$

$$F_T=\frac{1}{a^2\sin\theta}(K_H\sin\theta T_\theta)_\theta+(K_VT_z)_z, \quad (23)$$

where

$$K_H=l_H^2|D_s^2+D_T^2|^{\frac{1}{2}}, \quad K_V=l_V^2|u_z^2+v_z^2|^{\frac{1}{2}}, \quad (24)$$

$$D_s=a^{-1}\sin\theta(u/\sin\theta)_\theta, \quad D_T=a^{-1}\sin\theta(v/\sin\theta)_\theta. \quad (25)$$

The length scales l_H, l_V are of the order of $a\Delta\theta$ and Δz, respectively. For a dominantly free-atmosphere shear turbulence there is some justification, i.e., validity of the mixing-length hypothesis, for writing $l_H=C_Ha\Delta\theta$ and $l_V=C_V\Delta z$, where $0<C_H, C_V<1$ may be related to Kolmogoroff's universal constant. Since such an assumption cannot be made for a convective atmosphere, l_H and l_V will be determined by trial integrations.

A complete simulation of Jovian turbulence requires consideration of the form of the various "boundary" layers if l_H and l_V are to approach realistic values. The formulation (24) should not be extrapolated down to $z=0$ where $l\ll\Delta z$ and where constant stress and thermal boundary layers can form and which should have separate parameterizations. However, in view of the unknowns about the lower atmosphere such refinements are ignored and the same boundary conditions (12)–(14) are applied to (24). This will distort boundary layer properties but this role should be represented at least qualitatively.

At the upper boundary, $z=d$, some modification is required as the zero-stress condition gives $K_V=0$ at that level. This condition is not consistent with the thermodynamic condition that $T=0$ at that surface as the conductive transfer is now zero. To avoid a buildup of heat at $z=d$, a boundary conductivity K_B is introduced and the second term of (23) is rewritten as

$$[(K_V+K_B)T_z]_z, \quad (26)$$

with $K_B=0$ except at $z=d$, where

$$K_B=\frac{l_V^2}{\Delta z}|u^2+v^2|^{\frac{1}{2}}_{z=d}. \quad (27)$$

This seems to be a reasonable expression for K_B, being consistent with K_V and similar to the exchange coefficients used in meteorology. However, the form of K_B is not vital provided that its values are in a reasonable range. Physically it represents a small thermal boundary layer at the top of the atmosphere in which the eddy motion is small enough to exchange heat but not momentum, i.e., a thermoclinic layer. In a real atmosphere a radiative transfer term would provide a more realistic mechanism even though its role would be similar. This formulation of K_B allows us to maintain the model as a purely dynamical model that is related to the model of the previous sections.

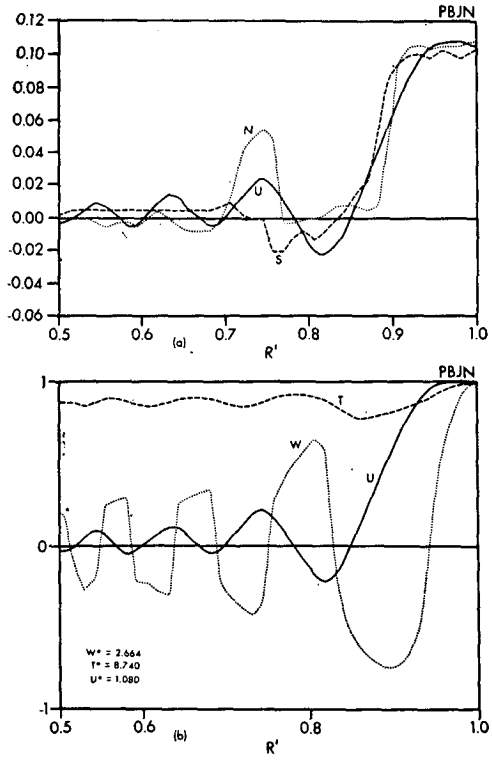

FIG. 18. Profiles of the most realistic solution PBJN. (a) Comparison of the predicted and observed variation with θ of u at $z=d$. Units are km sec^{-1}. U denotes the solution, N and S the mean Northern and Southern Hemisphere observed profiles after Chapman (1969). (b) Latitudinal profiles of the normalized variables, u/u^* at $z=d$ and T/T^*, w/w^* at $z=d/2$. Units are 10^{-4} km sec^{-1} for w, 10C for T, 10^{-1} km sec^{-1} for u.

d. Solution PBJN *for nonlinear diffusion*

Various integrations of the equations were made using the nonlinear diffusion coefficients, Eq. (24), and an assumed axisymmetry. Experimentation showed that a solution with the most realistic jet width and amplitude and matching phase positions[10] in the extra-equatorial extrema of u (Fig. 18a) is produced by the set of parameters:

Case PBJN: $\Delta T=135$K, $l_H=9618$ km ($\equiv 7a\Delta\theta$), $l_V=0.25$ km ($\equiv 0.1\Delta z$) with other variables being identical to those in case PBJ. The non-dimensional numbers had extremum values of $\mathrm{Ro}=5.6\times10^{-3}$, $\mathrm{Ta}=7.6\times10^4$, $d_E=0.27$, with the latter two numbers being based on the maximum $K_v=3.2\times10^{-3}$ km^2 sec^{-1} value; K_H has a maximum value of 1.6×10^3 km^2 sec^{-1}.

[An important point to note in making a comparison between an axisymmetric model and the Jovian atmo-

[10] In comparison with Northern Hemisphere data.

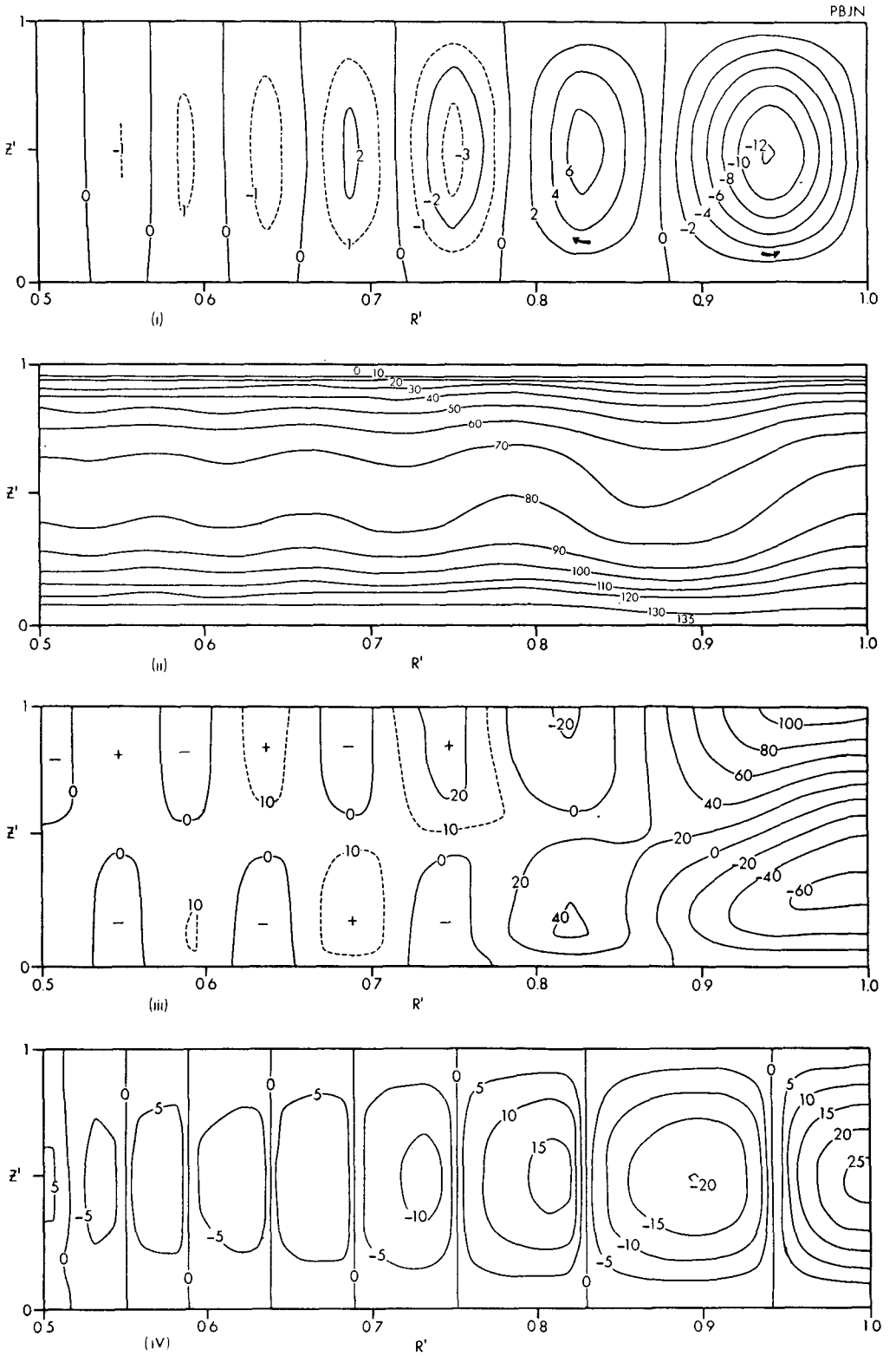

FIG. 19. Contours of the most realistic solution PBJN to simulate circulations in Jupiter's atmosphere: (i) $\psi \times 10$ [km^2 sec^{-1}]; (ii) T [°C]; (iii) u [m sec^{-1}]; (iv) w [cm sec^{-1}]. (Note change in units for this figure).

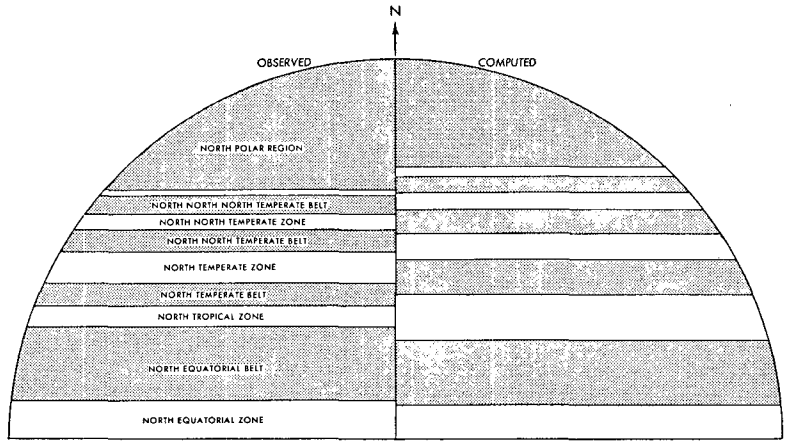

FIG. 20. Comparison of observed (left) and computed bands (right). Observations are from Michaux *et al.* (1967, p. 70), computed values from PBJN $w=0$ isopleths mapped with a foreshortening $\sin\theta$ factor.

sphere is that the Northern Hemisphere data must be regarded as the norm. This is because the Great Red Spot produces an anomalous (and non-axisymmetric) circulation in the Southern Hemisphere. Furthermore, a comparison of the u profile of the Southern Hemisphere data (Fig. 18a) and the solution SA8 (Fig. 6c) suggests that there may also be a latitudinal variation in the heating in the Southern Hemisphere.]

The flow profiles and contours of the solution PBJN are given in Figs. 18–20. The coincidence between the u profiles of the solution and the Northern Hemisphere data is good (Fig. 18a). The tropical jet is very similar to that produced by the linear viscosity model PBJ and is maintained by the same dynamics, but in extratropical regions greater realism in the u profile is achieved in the production of three strong secondary maxima and minima.

There are significant differences in the amplitudes of the secondary u extrema, particularly in that at $R'=0.74$. It is difficult to determine how seriously these differences should be taken in view of the uncertainties involved in the deduction of the observed profile. Because of the way the u field is examined, the observed profile reflects *maximum* atmospheric activity rather than the climatic mean. The squareness of the observed u profile could be a reflection of a squareness in the cloud tracer field, as suggested by the w solution, rather than being an intrinsic property of the u field. The observed profiles indicate a zonal velocity that is barotropically unstable, $B_{\max}\approx 6$, which suggests either that the observations are inaccurate or that non-axisymmetric effects are active. The solution PBJN is close to stability with $B_{\max}=1.02$ and its reaction to longitudinal disturbances will be discussed in Section 7.

The theoretical vertical velocity w (Figs. 18b and 19) contains five positive and four negative regions. These correspond well with the five zones and four belts which are semi-permanent features of Jupiter. The bands of the w solution and the planet appear to be coincident if the zones (light color) correspond to a $w>0$ region, i.e., upper level clouds, and the belts (dark color) correspond to $w<0$ regions. The differential rotation within the extra-equatorial bands is as observed.

It is difficult to compare the widths of the observed and the computed bands as the bands on the planet vary from decade to decade and there are no accurate estimates of the climatological w field. As a crude comparison, Fig. 20 contrasts the observed (or partially schematic) banded structure given by Michaux *et al.* (1967, p. 70) and that of the w solution. A general similarity is apparent between corresponding bands and in the narrowing of the bands with latitude up to the inactive polar region.

Even if the convective theory presented above is not applicable in its entirety to Jupiter, the agreement apparent in Fig. 20 strongly suggests that the cell structure on Jupiter is similar to that depicted by Fig. 19(i). If so, then the Jovian circulation cells are fairly uniform with the up and down branches of each cell covering equal areas. This result provides indirect evidence that the CISK mechanism cannot be active in the Jovian atmosphere for the circulations associated with that latent-heat-releasing mechanism are very asymmetric, the area of an upward branch being about one-fifth that of a down branch (Charney, 1970).

The square shape of the w profile (Fig. 18b) implies that the clouds will be uniform in intensity across each zone and cut off sharply at their edges. Although a large lateral mixing of turbulent elements could diffuse such a band structure, the presence of this type of basic w mode is needed to produce the highly orderly Jovian cloud structure. The polar region corresponds to a region of no mean vertical motion or a region of small scale incoherent motion.

Fig. 19(ii) shows that moderate thermal boundary layers form at the two horizontal surfaces, and that the

wave-like disturbance in T occurs mainly in the interior region (perhaps due to forcing by the $T=0$ upper boundary condition). Such boundary layers may be a feature of the real atmosphere but even so this solution is not so different from that of PBJ in which no layering occurs. This suggests that such layering does not qualitatively influence the basic character of the flow.

Finally, it must be noted that although the solution PBJN is realistic, a value of $l_H=7a\Delta\theta$ was used in its calculation. This mixing length is equal to about half the width of the tropical jet. Although disturbances are observed often of this length scale, they may be more characteristic of an upper level boundary layer than of the free atmosphere. The failure to constrain the parameterization to the subgrid-scale motions indicates a fundamental weakness in this calculation and the axisymmetric approximation.

Further calculations using a separate boundary layer formulation allow a reduction of l_H toward $a\Delta\theta$ while still giving realistic results. Such solutions (not shown) have pronounced boundary layers and an almost neutral interior lapse rate but the characteristics of the solution remain close to those of PBJN as regards cell scale and jet width. The production of a realistic cell scale seems to depend on having the crucial relative mixing factor $m=K_H/K_V$ equal to 10^6 in the free atmosphere. As formulation (24) covers boundary layer as well as the interior turbulence, K_V is too large in the interior. This then requires that a larger than desirable K_H (i.e., l_H) be used to achieve $m=10^6$. Although a separate boundary layer parameterization allows a lower K_V and then a lower l_H to be used in the interior, it appears that $l_H\approx a\Delta\theta$ is still a relatively large mixing length compared to $l_H\approx 10^{-1}a\Delta\theta$ normally used in shear turbulence calculations. In these calculations with $l_H\approx a\Delta\theta$ the equatorial zonal velocity is much smaller and the tropical jet no longer has a flat profile. To obtain a flat jet in this case we would probably have to perform 3-D integrations and allow longitudinal disturbances to develop to provide the large mixing implicit in the PBJN flow. Thus, a flow like PBJN that has such large mixing cannot, strictly speaking, be considered to be basically axisymmetric.

The characteristics of the PBJN flow in extra-equatorial regions have been made more realistic than those of PBJ by the scale-selective behavior of the nonlinear coefficients of the mixing length theory. Although the general characteristics and conclusions concerning the PBJN solution may be representative of the circulation dynamics, we must bear in mind the possibility that our parameterization is imitating the true cause and formulation, not representing it.

7. Concluding remarks

The realism of some of the solutions we have discussed suggests that they may provide a reasonable preliminary description of the Jovian circulations and that those motions may be a manifestation of large-scale organized convection. Correspondence between observation and theory occurred most closely for solution PBJN (Figs. 18–20). An understanding of this solution was built up from simpler solutions that examined the general properties of convection in a spherical gravity field.

The atmospheric flow suggested by solution PBJN consists of a series of elongated Bénard type rolls or "cyclic structures" forming five zones and four belts (Fig. 20). The square-shaped w variation with latitude produces a uniform cloud intensity and sharp zone boundaries. Strong horizontal turbulent mixing tends to diffuse the cloud bands. The bands decrease in intensity and width away from the equator. The polar region has no organized large-scale motion because of rotational suppression but it probably has disorganized small-scale activity.

Outside the equatorial bands, u and w are correlated in such a way (Fig. 18) that the equatorward side of zones ($w>0$) move in retrograde ($u<0$) and the poleward half moves positively ($u>0$). The opposite holds but to a lesser degree for the belts ($w<0$). This all corresponds with the observed differential rotation within the bands. It is worth noting that this differential rotation property is a basic feature of convection in a rotating system and does not depend on parameter values. The zonal velocity extrema coincide with the edges of the bands where $w=0$, and the maximum values of the barotropic instability criterion occurs at minimum u values and could lead to raggedness in the zones.

The zonal motion itself consists of a large positive upper level jet of 100 m sec^{-1} near the equator with a retrograde motion of 60 m sec^{-1} below it. Between these jets and the inactive polar region beginning at 45° are regions of alternating positive and negative zonal flow correlated with the banded structure. There is a general tendency in these alternating jets for the positive flows to be larger than the negative ones [Fig. 19(iii)]. These small upper level jets are countered by opposite flows directly below them.

Thermal "boundary" layers form at the top and bottom of the atmosphere where most of the small convective elements (parameterized as an eddy conductivity) exchange heat with the "boundaries." The vertical temperature gradient is weaker in the interior where the temperature has a horizontal wave-like form. Most of the vertical heat transport is produced by the motion in the equatorial region where warmer fluid rises to higher levels than elsewhere. This could produce a higher effective temperature for the equatorial region.

The temperature gradient and depth of the realistic solution PBJN were 135K and 50 km. However, similar solutions can be obtained at other depths with $\Delta T=135\text{K}\times 50/d$ for the range $20<d<500$ km; thus, the actual ΔT of our framework could lie in the range

$10<\Delta T<250$K, i.e., with a lapse rate of $0.02<\Delta T/d<12$K km^{-1}. The lower values of ΔT are to be favored as they provide a lower and more realistic heat loss from the planet and give lapse rates close to neutral. Unfortunately, the lower ΔT values are associated with the larger d values for which the Boussinesq model is less adequate. Thus, we are unable to make a definitive estimate of ΔT and d from the observed heat flux value with a Boussinesq model. For this, a non-Boussinesq model is needed.

The latitudinal velocity v achieves a maximum value of 7 m sec^{-1} at the upper surface. There are no estimates of the planetary v, probably due to its being small compared to u.

Although there seems to be no inconsistency between the observed and theoretical fields, it must be borne in mind that the theory is based on non-established hypotheses regarding the parameterization of the turbulence. Apart from trying to justify this formulation, there is a need to develop a hierachy of models towards a more complete parameterization. This seems desirable now that we have some idea of what must be parameterized and that realistic solutions can be expected. Even though boundary layer parameterization, radiative transfer, and non-Boussinesq effects need to be added for quantitative simulation, the main need is to formulate the role of the turbulence, and understanding this in just the Boussinesq framework is a desirable first step. We do not expect the flow in a non-Boussinesq model to be so different from that outlined above in that changes will be confined to the z variation with cells being distorted only in that direction. Hopefully, the latitudinal variation of the flow fields, upon which our observational comparisons are based, will be essentially unaltered.

Many of our solutions have shown that positive equatorial zonal motions can occur in an axisymmetric flow. The possibility or impossibility of such a feature has been discussed by Gierasch and Stone (1968) and Hide (1970). In our solutions such an equatorial flow is made possible by allowing a large lateral mixing of momentum from the jet at $R'=0.95$. Such a large mixing can only realistically be produced on Jupiter by large-scale longitudinal disturbances, in which case the actual atmospheric flow is not strictly definable as axisymmetric. In other words, an axisymmetric model can produce realistic solutions but under conditions which suggest that the real atmosphere is non-axisymmetric.

The axisymmetric jet does not peak exactly at the equator but has a region of maximum *angular velocity* at $R'=0.95$. To remove internal stresses by tending toward a state of solid rotation, the flow transports relative angular momentum toward latitudes of lower angular velocity; this follows from Eq. (20) when used in the angular momentum equation. This produces transfer toward the equator, i.e., against the angular momentum gradient, and maintains the equatorial flow. It should be noted that the observations do not demand that the jet peak right at the equator, only that the profile be fairly flat in the equatorial region. Although the jet at $R'=0.95$ is a basic feature of this type of convection and is not dependent on parameter values for its existence, the same is not true of the value of the zonal velocity at the equator which is dependent on the eddy viscosity value—but this may not be so when longitudinal variation is allowed and 3-D flow considered.

Subjecting the axisymmetric flows PBJ and PBJN to longitudinal perturbations through 3-D integrations indicated that although the convective amplitude is primarily axisymmetric, the flows themselves take on a cellular shape in the equatorial region (Fig. 21). The 3-D form of the equatorial cells is definitely due to convective instability as the flow remains barotropically stable. Now we know from 3-D calculations for a similar flow (case A2) that rolls are preferred at lower Rayleigh numbers in this system so that the axisymmetric solutions PBJ, PBJN are representative of a possible axisymmetric flow even though it cannot exist in itself at their parameter values. The slow growth rate of the 3-D cells out of the axisymmetric rolls ($\sim$100 hr) suggests that these parameter values lie close to the transition point of 2-D to 3-D flow. Thus, we expect that flows similar to PBJ, PBJN can exist but at lower Rayleigh numbers. Alternatively, recent observations by Keay *et al.* (1972) and Westphal (1969, and 1972 private communication) indicate the presence of equatorial hotspots on Jupiter very similar to the 3-D cells produced by the PBJN case so that the constrained axisymmetric flow and its subsequent breakdown may represent a more realistic picture of the lower atmosphere than the simpler axisymmetric state of the upper atmosphere.

In the 3-D integrations oval- and streak-shaped temperature anomalies occur. These must be due to convective instability as the unrealistically large mixing lengths suppress barotropic disturbances. A large cool temperature anomaly[11] comparable in shape and location to the Great Red Spot can be produced as an eddy[12] of an initially greatly disturbed axisymmetric PBJN flow. The disturbance is relatively short-lived because of the high viscosity used in the calculations. To achieve a satisfactory examination of Jovian flow requires that we perform multiple 3-D integrations using the nonlinear diffusion model with a separate boundary layer formulation and low values for the eddy coefficients. Such integrations will be discussed in a later paper.

Apart from the above calculation, we can also make some remarks about the actual Great Red Spot by considering what the solution PBJN reveals about its general environment. From the solution it appears that the South Tropical Zone in which the spot is embedded is a region of rising motion linked in cells to downward

[11] At $z=d/2$.

[12] A possibility suggested by Golitsyn (1970).

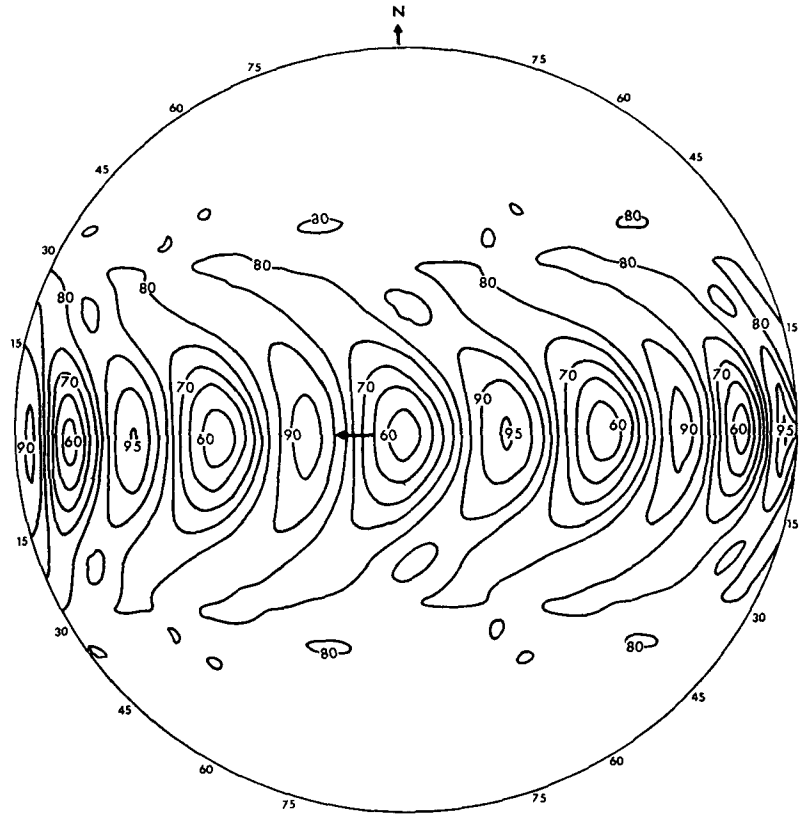

FIG. 21. Isotherms at $z=d/2$ at 5° intervals for the three-dimensional form of case PBJN. Solution is mapped onto an orthographic projection centered on the equator with periodicity over 60° of longitude. Flow is in equilibrium and arrow indicates retrograde direction of cell motion.

motion in the South Temperate Belt and the South Equatorial Belt. Compared with its Northern Hemisphere equivalent, the South Tropical Zone is very wide but the two corresponding belts have hemispheric differences (Michaux *et al.*, 1967). It is difficult to see how the mass conservation of the broader South Tropical Zone can be maintained by the narrow South Temperate Belt. Although the matter is not clear cut as the values of the velocity are not known for the zone, we can speculate that to maintain continuity it is necessary to have a downflow (or weaker upflow) by non-axisymmetric features, i.e., the Great Red Spot. The question of whether the South Tropical Zone has been broadened by the presence of the Great Red Spot or whether the Great Red Spot has been brought into existence by the broadening of the zone is a moot one. But, clearly, the mass conservation of the region in which it is embedded may provide clues and constraints for theories of the Great Red Spot.

In summary, it would appear that a simple gross explanation of Jupiter's circulation might be possible: that convective modes can produce the banded and jet-like elements, that ovals and streaks are the intrinsic shape of transient convective disturbance elements, and that solar heating effects (seasonal and diurnal) are secondary. These properties plus the predominant axisymmetry could make an understanding of Jupiter's atmosphere possible despite limited data, if the assumed dynamics is correct. (Unfortunately, the underlying scale-interaction mechanism is not understood.) The production of a large anomaly suggestive of the Great Red Spot in a simple system without complex features is possible but as yet only tentatively so. The small-scale thermal elements normally envisioned for convection may well be confined by the rotation of the planet to a lower thermal "boundary" layer and be unobservable. Only the large-scale motions traverse the whole atmosphere and do so mainly near the equator.

The procedure adopted in this study has been one of trying to find, for a given mode, the flow most consistent with the observations and then of asking ourselves whether the conditions under which such a flow occurs are meaningful. This process needs to be repeated for other possible modes, particularly that suggested by Stone (1967), so that the most realistic one can be isolated. Initially we must concentrate on basic modes

in the belief that the more fundamental a mode is, the greater is the probability of its occurrence.

APPENDIX

Numerical Techniques

1. Finite-difference equations

The method of integrating Eqs. (1)–(5) was adapted from that given in Williams (1969). Only variations from that method will be documented here and further details may be found in the earlier paper.

A staggered grid system, similar to that employed in the cylindrical geometry, is used for the spherical geometry. Velocity points are arranged around a central p, T point. The p, T points are placed at the intersection of latitude, longitude circles such that $\theta=(I-\frac{3}{2})\Delta\theta$, $\phi=(J-1)\Delta\phi$, $z=(K-\frac{3}{2})\Delta z$, where $I=1, 2, \ldots, L+1$; $J=1, 2, \ldots, M+1$; and $K=1, 2, \ldots, N+1$. The intervals between p points are given by $\Delta\theta=(\pi/2)/(I-1)$, $\Delta\phi=\Phi/(M-1)$, $\Delta z=d/(N-1)$ for a hemispheric domain of angular sector Φ in longitude. Radial velocity points lie on longitude circles through the p points and are located midway between the p points but at the same height. The w points lie on vertical lines through the p points, being midway between the p points. The u points lie on latitude circles through the p points, being midway between the p points in 3-D calculations but coincident with them in axisymmetric calculations.

Boundaries are placed midway between two extreme p points so that normal velocity points lie on them, providing a natural bias for boundary layers. At the pole, only a v boundary point is defined. This arrangement makes the computation straightforward as no singularities occur; this seems to be a useful feature of the staggered-grid system in spherical geometry.

The prediction equations are written in standard central difference notation as:

$$\delta_t\bar{u}^{t}+\frac{1}{R}\delta_\theta(\overline{\sin\theta v}^{\phi-\theta}\,\overline{u}^{\theta})+\frac{1}{R}\delta_\phi(\overline{u}^{\phi-\phi}\,\overline{u}^{\phi})+\delta_z(\overline{w}^{\phi-z}\,\overline{u}^{z})$$
$$=-\frac{1}{R}\delta_\phi p-\left(2\Omega+\frac{u}{R}\right)\times(\overline{\cot\theta\, v\sin\theta}^{\theta\phi}+\overline{w}^{z\phi}\sin\theta)+F_u, \quad \text{(A1)}$$

$$\delta_t\bar{v}^{t}+\frac{1}{R}\delta_\theta(\overline{\sin\theta v}^{\theta-\theta}\,\overline{v}^{\theta})+\frac{1}{R}\delta_\phi(\overline{u}^{\theta-\phi}\,\overline{v}^{\phi})+\delta_z(\overline{w}^{\theta-z}\,\overline{v}^{z})$$
$$=-\frac{1}{a}\delta_\theta p+[2\Omega+\overline{(u/R)}^{\theta\phi}]u\cos\theta-\frac{\overline{v}^{\theta z}}{a}+F_v, \quad \text{(A2)}$$

$$\delta_t\bar{w}^{t}+\frac{1}{R}\delta_\theta(\overline{\sin\theta v}^{z-\theta}\,\overline{w}^{\theta})+\frac{1}{R}\delta_\phi(\overline{u}^{z-\phi}\,\overline{w}^{\phi})+\delta_z(\overline{w}^{z-z}\,\overline{w}^{z})$$
$$=-\delta_z p+\beta g\bar{T}^{z}+\frac{\overline{v^2}^{\theta z}}{a}+[2\Omega+\overline{(u/R)}^{z\phi}]u\sin\theta+F_w, \quad \text{(A3)}$$

$$\delta_t\bar{T}^{t}+\frac{1}{R}\delta_\theta(\sin\theta v\bar{T}^{\theta})+\frac{1}{R}\delta_\phi(u\bar{T}^{\phi})+\delta_z(w\bar{T}^{z})=F_T, \quad \text{(A4)}$$

and the equation of mass conservation as

$$\delta_z w+\frac{1}{R}\delta_\theta(v\sin\theta)+\frac{1}{R}\delta_\phi u=0, \quad \text{(A5)}$$

where $R=a\sin\theta$. The equations are applied at the τ time level but the diffusion terms are evaluated at $\tau-1$.

The expressions for the linear diffusion terms are:

$$F_u=\frac{\nu_H}{a^2}\left(\bar{\nabla}_H^2 u-u\frac{\cos2\theta}{\sin^2\theta}+2\frac{\cot\theta}{\sin\theta}\delta_\phi\bar{v}^{\theta}\right)+\nu_V\delta_{zz}u, \quad \text{(A6)}$$

$$F_v=\frac{\nu_H}{a^2}\left(\bar{\nabla}_H^2 v-v\frac{\cos^2\theta}{\sin^2\theta}-2\frac{\cot\theta}{\sin\theta}\delta_\phi\bar{u}^{\phi}\right)+\nu_V\delta_{zz}v, \quad \text{(A7)}$$

$$F_w=\frac{\nu_V}{a^2}\bar{\nabla}_H^2 w+\nu_V\delta_{zz}w, \quad \text{(A8)}$$

$$F_T=\frac{\kappa_H}{a^2}\bar{\nabla}_H^2 T+\kappa_V\delta_{zz}T, \quad \text{(A9)}$$

where

$$\bar{\nabla}_H^2 q\equiv\frac{1}{\sin\theta}\delta_\theta(q\sin\theta)+\frac{1}{\sin^2\theta}\delta_{\phi\phi}q. \quad \text{(A10)}$$

The nonlinear diffusion terms were taken in the form

$$F_u=\frac{1}{a\sin^2\theta}\delta_\theta(K_H^a\sin^2\theta D_s)-\frac{1}{a\sin\theta}\delta_\phi(K_H^b D_T)+\delta_z(K_V^a\delta_z u), \quad \text{(A11)}$$

with

$$K_H^a=l_H^2\left|D_s^2+\overline{D_T^2}^{\theta\phi}\right|^{\frac{1}{2}},\quad K_H^b=l_H^2\left|\overline{D_s^2}^{\theta\phi}+D_T^2\right|^{\frac{1}{2}},$$
$$K_V^a=l_V^2\left|D_u^2+\overline{D_v^2}^{\theta\phi}\right|^{\frac{1}{2}},$$

$$F_v=\frac{1}{a\sin^2\theta}\delta_\theta(K_H^c\sin^2\theta D_T)+\frac{1}{a\sin\theta}\delta_\phi(K_H^d D_s)+\delta_z(K_V^b\delta_z v), \quad \text{(A12)}$$

† This unusual form is necessary to provide conservation of kinetic energy and angular momentum.

with

$$K_H^c = l_H^2 \left| \frac{\overline{\quad}^{\theta\phi}}{D_s^2} + D_T^2 \right|^{\frac{1}{2}}, \quad K_H^d = l_H^2 \left| D_s^2 + \overline{D_T^2}^{\theta\phi} \right|^{\frac{1}{2}},$$

$$K_V^b = l_V^2 \left| \overline{D_u^2}^{\theta\phi} + D_v^2 \right|^{\frac{1}{2}},$$

and

$$F_T = \frac{1}{a^2 \sin\theta} \delta_\theta (K_H^e \sin\theta \delta_\theta T) + \frac{1}{a^2 \sin^2\theta} \delta_\phi (K_H^f \delta_\phi T) + \delta_z (K_V^c \delta_z T), \quad \text{(A13)}$$

with

$$K_H^e = l_H^2 \left| \frac{\overline{\quad}^{\phi}}{D_s^2} + \overline{D_T^2}^{\theta} \right|^{\frac{1}{2}}, \quad K_H^f = l_H^2 \left| \overline{D_s^2}^{\theta} + \overline{D_T^2}^{\phi} \right|^{\frac{1}{2}},$$

$$K_V^c = l_V^2 \left| \overline{D_u^2}^{\phi} + \overline{D_v^2}^{\theta} \right|^{\frac{1}{2}},$$

where

$$\left.\begin{aligned} &l_H = C_H a \Delta\theta, \quad l_V = C_V \Delta z \\ &D_s = \frac{\sin\theta}{a} \delta_\theta (u/\sin\theta) + \delta_\phi (v/a \sin\theta) \\ &D_T = \frac{\sin\theta}{a} \delta_\theta (v/\sin\theta) - \delta_\phi (u/a \sin\theta) \\ &D_u = \delta_z u, \quad D_v = \delta_z v \end{aligned}\right\}$$

are related to the rates of strain.

The strain terms are staggered in space also. This is because in the basic Navier-Stokes equations, the strains e_{ij} must be correctly staggered if the finite-difference equivalent of the energy molecular transform equation [see, e.g., Eq. (20) of Williams (1971)] is to give accurate dissipation estimates. Thus, normal strains e_{ii} are defined at p points and tangential strains e_{ij} are defined at the intersecting corners of the i,j coordinates. The arrangement reflects the molecular functioning of the fluid and the nature of pressure in the basic Navier-Stokes derivation. If the strain functions are incorrectly staggered, the dissipation can be strongly enhanced.

The time iteration of Eqs. (A1)–(A4) is accompanied by the solving of the following Poisson equation for p to satisfy (A5) implicitly:

$$\frac{1}{aR} \delta_\theta (\sin\theta \delta_\theta p) + \frac{1}{R^2} \delta_{\phi\phi} p + \delta_{zz} p = \frac{1}{R} \delta_\theta (\sin\theta GV) + \frac{1}{R} \delta_\phi (GU) + \delta_z (GW), \quad \text{(A14)}$$

where GU, GV, GW denote the various components of the prediction equations. Eq. (A14) can be solved efficiently using trigonometric series expansions in ϕ and z in exactly the same way as for the cylindrical case of Williams (1969). This similarity is produced by the shallow atmosphere approximation.

The time step Δt used for the planetary-scale calculations was of the order of 200 sec, being determined by the diffusion criterion. The need to take smaller time steps because of the small grid lengths near the pole can be avoided by selective scale filtering (see, e.g., Holloway *et al.*, 1972). However, Jupiter seems to be inactive beyond 45° latitude so integrations can be terminated at that latitude and any Δt problem avoided. For axisymmetric flow there is no problem.

2. Some numero-physical limitations

The equation system (A1)–(A4) with (A14) was chosen initially in the hope that its three-dimensional form would provide a generalized model for investigating both shallow and deep non-hydrostatic atmospheres. However, in calculations for very shallow or highly hydrostatic fluid layers the apparently general 3-D Navier-Stokes equations become unsuitable for calculation on certain computers unless they are modified.

The analysis of what happens when d/L is decreased can be made either physically through a scale analysis or numerically through accuracy and error analyses. The latter procedure is taken so that the limitations can be quantitatively defined. The problem arises in two areas: 1) in the prediction equation $w_t = p_z + GW$, w becomes small as d/L decreases so that w_t becomes of the order of the roundoff error and the two other terms become mutually balancing, i.e., hydrostatic balance is reached; 2) in the Poisson equation the two vertically differentiated terms p_{zz} and GW_z dominate the equation, resulting in large errors in the predicted horizontal variation of p.

The degeneracy of the Poisson equation occurs rapidly as $(d/L)^2$; for example, for a machine accuracy of 1×10^{-8}, the error in solving the Poisson equation is only 2×10^{-7} for $d/L=1$ but becomes 2×10^{-4} for $d/L=1/100$ and 1×10^{-1} for $d/L=1/1000$. Thus, $d/L=1/1000$ is about the limit of the 3-D method for this level of machine accuracy. Needless to say, this limitation is machine-dependent and would be less, say, for a CDC 6600 than a UNIVAC 1108. With 1108 double precision, i.e., an accuracy of 1×10^{-16}, the Poisson equation can be solved accurately down to $d/L=10^{-8}$ where the error is 4×10^{-2}. Thus, the limitation can be overcome for most practical purposes. However, for single-precision 1108 calculations, inaccuracies reach a serious level for the very shallow Joviana tmosphere where $d/L=1/1000$. For the Earth's atmosphere the problem could be ignored.

A similar problem occurs with the horizontal grid points when the pole is approached. There compression

of grid points produces a ratio

$$(L_\phi/L_\theta)^2=(a\sin\theta\Delta\phi/a\Delta\theta)^2=\Delta\phi^2/4=10^{-3}$$

in the staggered grid system. The problem is not serious as the solutions are still accurate. The problem is acute in the non-staggered grid system where $\sin\theta=0$ occurs.

Although for small d/L the hydrostatic approximation can be made and a simpler numerical scheme constructed, it would have little computational advantage over the then slightly redundant 3-D scheme. As we require a general model to investigate deep and shallow atmospheres and intermediate ones, we prefer just to modify the 3-D scheme when applying it to very shallow system $[d/L\approx O(10^{-3})]$. The computational procedure resembles that used in ocean circulation calculations (Bryan, 1969) and its validity has been confirmed by comparing its solutions with those obtained by the standard 3-D method in double precision.

To illustrate the procedure consider the simple two-dimensional system of equations

$$v_t=-\pi_x+GV,\quad w_t=-\pi_z+GW,\quad \mathfrak{D}=v_x+w_z=0. \tag{A15}$$

Solving $\nabla^2 p=\nabla\cdot\mathbf{G}$ for this system for small $(d/L)^2$ gives a quasi-hydrostatic pressure p^s. Let $p^s=p^c+\epsilon(x)$, where p^c is the correct pressure and $\epsilon(x)$ the x-varying pressure deficiency. The deficiency $\epsilon(x)$ enters when a prediction is made for v, i.e., $v_t^s=-p_x^s+GV=-p_x^c-\epsilon_x+GV$, so that $v_t^c=v_t^s+\epsilon_x$, where v^c is the correct v. Using the fact that $\epsilon(x)$ is independent of z for small $(d/L)^2$, it can be obtained by averaging the equation over z, i.e., $\bar{v}_t^s=-\epsilon_x$ as $\bar{v}^c=0$. Then $v^c=v^s-\bar{v}^s$ gives the correct v and the p field can be adjusted. The correct w field can be obtained by integrating $w_z=-v_x^c$. This simple procedure can be extended to three dimensions by solving a two-dimensional Poisson for ϵ.

3. Some alternatives in solving the Navier-Stokes equations

1) In the method discussed by Williams (1969), prediction equations are used for all three velocity components (u,v,w). It is slightly more accurate to obtain w, for example, by integrating the conservation equation. Values of the divergence $\mathfrak{D}$ are then zero everywhere except at $z=d-(\Delta z/2)$, but values there are kept small by the procedure of D_t adjustment in the Poisson solution. But now the adjustment is only made at $z=d-(\Delta z/2)$. The result is that with $\mathfrak{D}=0$ practically everywhere then quadratic conservation properties, etc., are improved.

2) The zero'th mode of the pressure eigenfunctions can be obtained from the vertically averaged pressure field more aesthetically than by direct integration (see Williams, 1969, Section 6e). For convenience consider an eigenfunction expansion to a 2-D Poisson equation:

$$p=\sum_\beta p_\beta H_\beta(z). \tag{A16}$$

Averaging over z gives the zero'th mode as $p_0=N^{-1}\bar{p}$ where N is the number of eigenfunctions. Thus, p_0 can be obtained from p via the averaged equation of motion

$$\bar{p}_r=\overline{GV}-\bar{v}_t, \tag{A17}$$

which in the finite-difference form

$$\delta_r\bar{p}=\overline{GV}+\frac{\bar{v}_{\tau-1}}{2\Delta t} \tag{A18}$$

ensures that $\bar{D}_t=0$. Unlike the degenerate Poisson equation for p_0, Eq. (A17) does not lose information in GV through its differentiation and the integral constraint (44) of Williams (1969) is achieved directly.

3) The boundary conditions on p can be met by introducing simple auxiliary pressures. For Eqs. (A15), for example, these would be defined as

$$pw=\int_0^z GW\,dz,\quad pv=\int_0^x GV\,dx, \tag{A19}$$

with boundary values given by $pw_z=GW$, $pv_z=0$ on $z=0$, d and $pv_x=GV$, $pw_x=0$ on $x=0$, L. Then writing $p=pv+pw+p^*$, the Poisson equation becomes

$$\nabla^2 p^*=-pw_{xx}-pv_{zz}, \tag{A20}$$

with simpler boundary conditions of p_x^*, $p_z^*=0$. The equations of motion reduce to

$$u_t=-(p^*+pw)_x,\quad w_t=-(p^*+pv)_z. \tag{A21}$$

Acknowledgments. We are grateful to Clark R. Chapman for providing us with some of his original graphs and to Philip G. Tunison for his invaluable drafting. We greatly appreciate the advice and comments given us on this work by R. E. Danielson, C. T. Gordon, F. B. Lipps and S. Manabe.

REFERENCES

Aumann, H. H., C. M. Gillespie and F. J. Low, 1969: The internal powers and effective temperatures of Jupiter and Saturn. *Astrophys. J.*, **157**, L69-L72.

Bryan, K., 1969: A numerical method for the study of the circulation of the world ocean. *J. Comput. Phys.*, **4**, 347–376.

Busse, F. H. 1970: Differential rotation in stellar convection zones. *Astrophys. J.*, **159**, 629–639.

Chandrasekhar, S., 1961: *Hydrodynamic and Hydromagnetic Stability.* Oxford University Press, 652 pp.

Chapman, C. R., 1969: Jupiter's zonal winds: Variation with latitude. *J. Atmos. Sci.*, **26**, 986–990.

Charney, J. G. 1970: Tropical cyclogenesis and the formation of the intertropical convergence zone. *Mathematical Problems in the Geophysical Sciences*, W. H. Reid, Ed., Providence, R. I., Amer. Math. Soc., 355–368.

——, and A. Eliassen 1965: On the growth of the hurricane depression. *J. Atmos. Sci.*, **21**, 68–75.

Deardorff, J. W., 1971: On the magnitude of the subgrid scale eddy coefficient. *J. Comput. Phys.*, **7**, 120–133.

——, and G. E. Willis, 1967: Investigation of turbulent thermal convection between horizontal plates. *J. Fluid Mech.*, **28**, 675–704.

Eady, E. T., 1949: Long waves and cyclone waves. *Tellus*, **1**, 33–52.

Gierasch, P. J., 1970: The fourth Arizona conference on planetary atmospheres: Motions of planetary atmospheres. *Earth Extraterr. Sci.*, **1**, 171–184.

– – –, and P. H. Stone, 1968: A mechanism for Jupiter's equatorial acceleration. *J. Atmos. Sci.*, **25**, 1169–1170.

Gilman, P. A., 1972: Boussinesq convective model for large scale solar circulations. Manuscript, NCAR, Boulder, Colo.

Golitsyn, G. S., 1970: A similarity approach to the general circulation of planetary atmospheres. *Icarus*, **13**, 1–24.

Hide, R., 1969: Dynamics of the atmospheres of the major planets. *J. Atmos. Sci.*, **26**, 841–853.

——, 1970: Equatorial jets in planetary atmospheres. *Nature*, **225**, 254.

Hinze, J. O., 1959: *Turbulence*. New York, McGraw-Hill, 586 pp.

Holloway, J. L., M. J. Spelman and S. Manabe, 1972: A latitude-longitude grid suitable for a numerical time-integration of a global circulation model. *Mon. Wea. Rev.*, **101**, 69–78.

Ingersoll, A. P., and J. N. Cuzzi, 1969: Dynamics of Jupiter's cloud bands. *J. Atmos. Sci.*, **26**, 981–985.

Keay, C. S. L., F. J. Low and G. H. Ricke, 1972: Infrared maps of Jupiter. *Sky Telescope*, **44**, 296–297.

Kraichnan, R. H., 1962: Turbulent thermal convection at arbitrary Prandtl number. *Phys. Fluids*, **5**, 1374–1389.

——, 1964: Direct-interaction approximation for shear and thermally driven turbulence. *Phys. Fluids*, **7**, 1048–1062.

Kuo, H. L., 1949: Dynamic instability of two-dimensional nondivergent flow in barotropic atmosphere. *J. Meteor.*, **6**, 105–122.

Lau, H. E., 1913: Uber die Rotation des Planeten Jupiter. *Astron. Nachr.*, **195**, 313.

Lewis, J. S., 1969: The clouds of Jupiter and the NH_3–H_2O and NH_3–H_2S systems. *Icarus*, **10**, 365–378.

Michaux, C. M., *et al.*, 1967: *Handbook of the Physical Properties of the Planet Jupiter*. NASA SP-3031, Gov't. Printing Office, Washington, D. C.

Ooyama, K., 1969: Numerical simulation of the life cycle of tropical cyclones. *J. Atmos. Sci.*, **26**, 3–40.

Peek, B. M., 1958: *The Planet Jupiter*. London, Faber and Faber, 288 pp.

Phillips, N. A., 1966: The equations of motion for a shallow rotating atmosphere and the "traditional approximation." *J. Atmos. Sci.*, **23**, 626–628.

——, 1968: Reply to Veronis' comments. *J. Atmos. Sci.*, **25**, 1155–1157.

Rivas, E. E., 1971: The circulation of the atmosphere of Venus. Ph.D. thesis, Dept. of Meteorology, M. I. T.

Roberts, P. H. 1968: On the thermal instability of a rotating-fluid sphere containing heat sources. *Phil. Trans. Roy. Soc. London*, **A263**, 93–117.

Rossby, H. T., 1969: A study of Bénard convection with and without rotation. *J. Fluid Mech.*, **36**, 309–335.

Smagorinsky, J., 1963: General circulation experiments with the primitive equations. *Mon. Wea. Rev.*, **91**, 99–164.

Spiegel, E. A., 1966: Energy transport by turbulent convection. *Stellar Evolution*, Stein and Cameron, Eds., New York, Pergamon Press, 143–147.

——, 1971: Convection in stars. *Ann. Rev. Astron. Astrophys.*, **9**, 323–352.

Stone, P. H., 1967: An application of baroclinic stability theory to the dynamics of the Jovian atmosphere. *J. Atmos. Sci.*, **24**, 642–652.

——, 1972a: A simplified radiative-dynamical model for the static stability of rotating atmospheres. *J. Atmos. Sci.*, **29**, 405–418.

——, 1972b: On non-geostrophic baroclinic stability: Part III. The momentum and heat transports. *J. Atmos. Sci.*, **29**, 419–426.

Trafton, L. M., and R. L. Wildey, 1970: Jupiter: His limb darkening and the magnitude of his internal heat source. *Science*, **168**, 1214–1215.

Veronis, G., 1968: Comments on Phillips' proposed simplification of the equations of motion for a shallow rotating atmosphere. *J. Atmos. Sci.*, **25**, 1154–1155.

Wasiutynski, J., 1946: Studies in hydrodynamics and structure of stars and planets. *Astrophys. Norv.*, **4**, 1–497.

Westphal, J. A., 1969: Observations of localized 5-micron radiation from Jupiter. *Astrophys. J.*, **157**, L63-L64.

Williams, G. P. 1969: Numerical integration of the three-dimensional Navier-Stokes equations for incompressible flow. *J. Fluid Mech.*, **37**, 727–750.

——, 1971: Baroclinic annulus waves. *J. Fluid Mech.*, **49**, 417–449.

——, 1972: Friction term formulation and convective instability in a shallow atmosphere. *J. Atmos. Sci.*, **29**, 870–876.